

## Part III - Ch 4 Ship-waterway and ship-ship interactions

Verheij, H.J.; van der Hout, A.J.; Koedijk, O.C.; van Koningsveld, M.; de Vriend, H.J.

**Publication date**

2021

**Document Version**

Final published version

**Published in**

Ports and Waterways

**Citation (APA)**

Verheij, H. J., van der Hout, A. J., Koedijk, O. C., van Koningsveld, M., & de Vriend, H. J. (2021). Part III - Ch 4 Ship-waterway and ship-ship interactions. In M. V. Koningsveld, H. J. Verheij, P. Taneja, & H. J. de Vriend (Eds.), *Ports and Waterways: Navigating a changing world* (pp. 301-346). TU Delft OPEN Publishing.

**Important note**

To cite this publication, please use the final published version (if applicable). Please check the document version above.

**Copyright**

Other than for strictly personal use, it is not permitted to download, forward or distribute the text or part of it, without the consent of the author(s) and/or copyright holder(s), unless the work is under an open content license such as Creative Commons.

**Takedown policy**

Please contact us and provide details if you believe this document breaches copyrights. We will remove access to the work immediately and investigate your claim.

## 4 Ship-waterway and ship-ship interactions

<sup>1</sup>Sailing ships influence the bed and banks of navigation channels and vice versa. The same goes for the sailing behaviour of other ships. This chapter deals with these interactions.

A ship sailing with a certain speed will displace an amount of water. The ship's bow will constantly push water to the front, aside and downwards, and a corresponding amount of water returns behind the stern. This induces a so-called return current along and under the ship, against the sailing direction. The return current induces a water-level depression around the ship. This must be kept in mind when calculating the water depth under the keel or [Under Keel Clearance \(UKC\)](#), otherwise the ship may run aground.



Figure 4.1: Primary, secondary and propeller jet water motion (by TU Delft – Ports and Waterways is licenced under CC BY-NC-SA 4.0).

The ship-induced water motion (see [Figure 4.1](#)) is composed of a primary and a secondary component, as well as jets from propellers and thrusters. The primary water motion is linked directly to the water displacement by the ship and consists of the return current and the accompanying water level depression. Looking at it from a fixed point, the primary motion is a (forced, long) wave, since it moves along with the ship and extends over its entire length.

The secondary water motion consists of ship-induced (free, short) waves. The height of these waves is strongly determined by the speed of the ship, but also depends on the ship's main dimensions and the hull shape. Furthermore, the secondary water motion depends on the primary one. The ship-induced waves will increase as the ship speed increases, and as the return current and the water level depression decrease. This explains why smaller and faster ships usually cause bank erosion by secondary waves; larger and slower ships by the return current.

---

<sup>1</sup>This chapter made use of 'Inland Waterways. Ports, Waterways and Inland Navigation' ([Verheij et al., 2008](#)) and 'Capacities of Inland Waterways' ([Groenvelde et al., 2006](#)), lecture notes for the Ports and Waterways courses CIE4330 and CIE5306 at TU Delft, respectively.

The third component, the jets of bow thrusters and main propellers, may cause bed and bank erosion and exert forces on nearby structures.

In this chapter we will first discuss the primary and secondary water motion, and then the jets induced by propulsion systems. We will furthermore discuss some specific aspects of the induced water motions, and consider the net result of propulsion and resistance: the ship speed. Finally, we will show some applications of CFD models to ship-induced hydrodynamics. Most of the information provided is based on Dutch research and published in the M1115 reports of [Delft Hydraulics \(1988\)](#) or Rock Manual ([CIRIA; CUR; CETMEF, 2007](#)). Another important source of information is the BAW manual ([BAW, 2011](#)), which is based on research in Germany.

Within the framework of prevailing rules and regulations (see, for instance, [RVW, 2020](#)) ship-induced water motions determine the design of waterways, in particular the required bed and bank protections.

## 4.1 Primary water motion

The primary water motion can be explained from Bernoulli's theorem and the equation of continuity. These equations, rewritten in terms of energy conservation, were formulated and solved analytically by [Schijf \(1949\)](#) (also see [Janssen and Schijf, 1953](#)). Schijf also found proof for the so-called natural limit speed for ships, which we will also discuss. [Bouwmeester \(1977\)](#) derived the return current and the water level depression from a momentum conservation principle (which Bernoulli's theorem basically is). We will briefly discuss this alternative approach. In Germany, the derivation by Schijf is attributed to [Thiele \(1901\)](#) and [Krey \(1913\)](#).

The water motion around sailing vessels is very complicated, particularly because of the three-dimensional current pattern next to and underneath the ship and along the hull. With respect to the resistance experienced, the shape of most inland vessels is not ideal, due to their large amidships cross-section and their large block coefficient. Furthermore, the limited width and depth of inland waterways play an important role in the water motion.

As mentioned in the introduction, the return current causes a depression of the water level around the ship, causing a sinkage of the ship of approximately the same magnitude. This sinkage is mostly combined with a positive trim, due to the water level depression caused by the propeller jet.

### 4.1.1 Energy conservation approach

Assume the three-dimensional flow can be simplified to one-dimensional, that the ship's sinkage is equal to the water-level depression, and that the ship has no trim. In that case there is an exact analytical solution. Furthermore, we assume:

- a straight, infinitely long prismatic channel section;
- a prismatic shape of the ship (i.e. the cross-section amidships applies over the entire length);
- a constant speed of the ship;
- the course of the ship is strictly parallel to the channel axis;
- a uniform return current over the entire wet channel profile, beside as well as below the ship;
- a uniform water level depression over the entire channel width;
- no energy losses, i.e. shear stress and inertial losses are neglected;
- no influence of ship-initiated waves or phenomena caused by helical motion.

Taking a Lagrangian approach, we fix the co-ordinate system to the ship. This means that the undisturbed water is apparently flowing with velocity  $V_s$  against the ship's sailing direction ([Figure 4.2](#)). Alongside and under the ship the velocity will become equal to  $(V_s + U_r)$ .

Using Bernoulli's theorem between cross-sections I and II in [Figure 4.2](#), considering the total head  $H = h_0 + \frac{V_s^2}{2g}$  and  $h_I - h_{II} = z$ , gives:

$$z = \frac{(V_s + U_r)^2}{2g} - \frac{V_s^2}{2g} = \frac{V_s U_r}{g} + \frac{U_r^2}{2g} \quad (4.1)$$

Continuity between cross-section I and II requires (for explanation of symbols also see Figure 4.3):

$$Q = V_s A_c = (V_s + U_r)(A_c - A_s - W_s z) \quad (4.2)$$

in which:

- $A_c$  =  $W_s h_0$  = wet cross-sectional area of the undisturbed channel [m<sup>2</sup>]
- $A_s$  =  $B_s D_s$  = ship's underwater cross-section amidships [m<sup>2</sup>]
- $h_0$  = undisturbed water depth in the channel [m]
- $W_s$  = undisturbed channel width at the water surface [m]
- $B_s$  = the ship's beam [m]
- $D_s$  = draught of the ship [m]
- $V_s$  = ship speed [m/s]
- $z$  = maximum water-level depression [m]
- $U_r$  = maximum return current velocity along the ship [m/s]

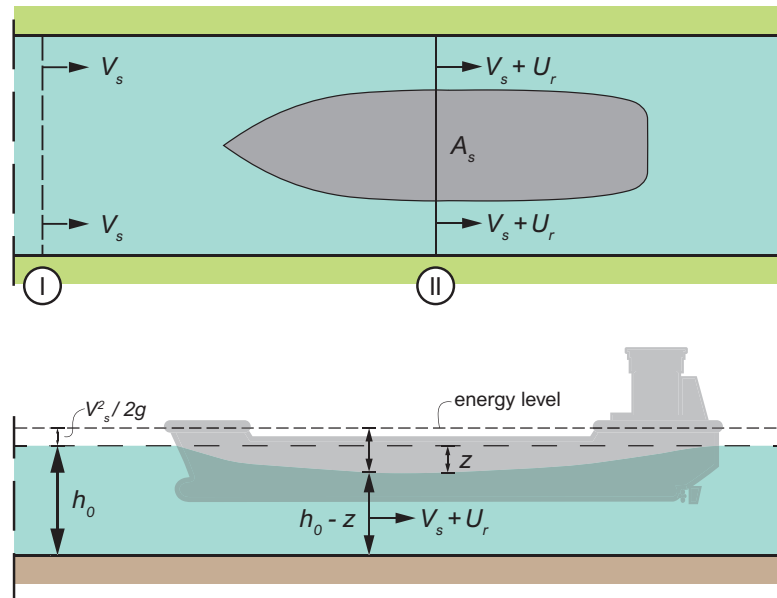


Figure 4.2: Relative water motion in a ship-fixed coordinate system (by TU Delft – Ports and Waterways is licenced under CC BY-NC-SA 4.0).

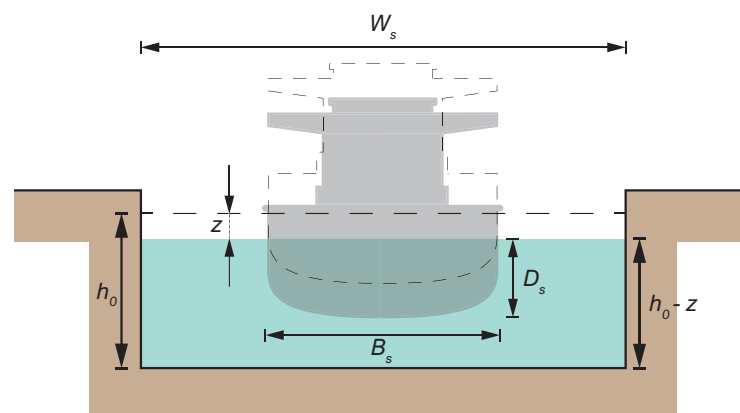


Figure 4.3: Definition of symbols at the cross-section amidships (by TU Delft – Ports and Waterways is licenced under CC BY-NC-SA 4.0).

### Limit speed

The depth and width restrictions of the waterway influence the speed of the ship. Schijf developed a method based on energy conservation to compute the natural limit speed. This speed is the maximum possible sailing speed ( $V_{lim}$ ) for a certain ship in a restricted waterway of given dimensions. Schijf's approach applies to shallow water conditions.

According to Schijf, the limit speed of a ship is reached when the return current has become critical, i.e. the Froude number equals 1. When the ship's speed would further increase, the water motion next to the ship would become supercritical and the water depth would jump to a much smaller value. In that case, the continuity condition is not be satisfied any more, despite the higher current velocity. Consequently, water will accumulate in front of the bow, to the extent that a self-propelled ship is not able to overcome this. Sailing yachts and ships tugged from the banks are able to go faster, since they are not self-propelled. Schijf's method is therefore restricted to self-propelled ships.

Using Equation 4.2 to replace  $V_s + U_r$  in Equation 4.1, realising that  $A_c/W_s = \bar{h}$  and dividing by  $\bar{h}$  we can derive the dimensionless:

$$\left(\frac{z}{\bar{h}}\right)^3 + \left(\frac{z}{\bar{h}}\right)^2 \left[ \frac{Fr_h^2}{2} - 2 \left(1 - \frac{A_s}{A_c}\right) \right] + \frac{z}{\bar{h}} \left[ \left(1 - \frac{A_s}{A_c}\right)^2 - Fr_h^2 \left(1 - \frac{A_s}{A_c}\right) \right] - Fr_h^2 \frac{A_s}{A_c} \left(1 - \frac{1}{2} \frac{A_s}{A_c}\right) = 0 \quad (4.3)$$

after some rearranging, in which  $\bar{h} = A_c/W_s$  is the mean channel depth and  $Fr_h^2 = V_s^2/g\bar{h}$ . From this equation  $z$  can be solved, and subsequently  $U_r$  from Equation 4.2.

If the ship sails at its limit speed,  $V_s = V_{lim}$ , and Equation 4.1 yields:

$$V_{lim} + U_r = \sqrt{V_{lim}^2 + 2gz} \quad (4.4)$$

whence, according to Equation 4.2,

$$Q = (V_{lim} + U_r)(A_c - A_s - W_s z) = \sqrt{V_{lim}^2 + 2gz} (A_c - A_s - W_s z) \quad (4.5)$$

This expresses  $Q$  as a function of  $z$ , so the value  $z_{lim}$  at which the maximum discharge occurs is found by setting  $dQ/dz = 0$ . This is the case for

$$\frac{z_{lim}}{\bar{h}} = \frac{1}{3} \left(1 - \frac{A_s}{A_c} - \frac{V_{lim}^2}{g\bar{h}}\right) \quad (4.6)$$

The corresponding maximum discharge follows from substitution of Equation 4.6 into Equation 4.5, to yield:

$$Q_{max} = \sqrt{V_{lim}^2 + \frac{2}{3}g\bar{h} \left(1 - \frac{A_s}{A_c} - \frac{V_{lim}^2}{g\bar{h}}\right)} A_c \left[1 - \frac{A_s}{A_c} - \frac{1}{3} \left(1 - \frac{A_s}{A_c} - \frac{V_{lim}^2}{g\bar{h}}\right)\right] \quad (4.7)$$

or, after some rearranging,

$$\frac{Q_{max}}{A_c \sqrt{g\bar{h}}} = \left[ \frac{2}{3} \left(1 - \frac{A_s}{A_c} + \frac{1}{2} \frac{V_{lim}^2}{g\bar{h}}\right) \right]^{\frac{3}{2}} \quad (4.8)$$

Since  $Q_{max} = V_{lim} A_c$  this means that

$$\frac{V_{lim}}{\sqrt{g\bar{h}}} = \left[ \frac{2}{3} \left(1 - \frac{A_s}{A_c} + \frac{1}{2} \frac{V_{lim}^2}{g\bar{h}}\right) \right]^{\frac{3}{2}} \quad (4.9)$$

whence:

$$\left(\frac{V_{lim}}{\sqrt{gh}}\right)^2 - 3\left(\frac{V_{lim}}{\sqrt{gh}}\right)^{\frac{2}{3}} + 2\left(1 - \frac{A_s}{A_c}\right) = 0 \quad (4.10)$$

from which  $V_{lim}$  can be solved.

In the trivial case  $A_s/A_c = 1$  (the ship fills the entire channel cross-section) the solution is as expected:  $V_{lim} = 0$ . In the extreme case of  $A_s/A_c = 0$  the solution is  $V_{lim} = \sqrt{gh}$ . So in infinitely wide, shallow water a ship's maximum speed is equal to the celerity of a shallow water wave. In most inland waterways  $A_s/A_c$  lies between 0.1 and 0.3.

Around a ship sailing at the limit speed the Froude number can be defined as

$$Fr_{lim} = \frac{V_{lim} + U_{lim}}{\sqrt{gh\left(1 - \frac{A_s}{A_c} - \frac{z_{lim}}{h}\right)}} \quad (4.11)$$

One may claim that this is the Froude number that becomes equal to 1 in case of the limit speed, but in practice one uses  $Fr_{lim} = V_{lim}/\sqrt{gh} = 1$ . If the Froude number according to Equation 4.11 is set equal to 1, this means that

$$\frac{U_{lim}}{\sqrt{gh}} = \sqrt{1 - \frac{A_s}{A_c} - \frac{z_{lim}}{h}} - \frac{V_{lim}}{\sqrt{gh}} = \sqrt{\frac{2}{3}\left(1 - \frac{A_s}{A_c}\right) + \frac{1}{3}\frac{V_{lim}^2}{gh}} - \frac{V_{lim}}{\sqrt{gh}} \quad (4.12)$$

in which we have used Equation 4.6.

Figure 4.4 shows  $V_{lim}/\sqrt{gh}$  (Equation 4.10),  $z_{lim}/h$  (Equation 4.6) and  $U_{lim}/\sqrt{gh}$  (Equation 4.12) as functions of  $A_s/A_c$ . Apart from the limit speed associated with the return current and the water level depression, there is another limit speed associated with the secondary water motion. In the next section we will derive an expression for it.

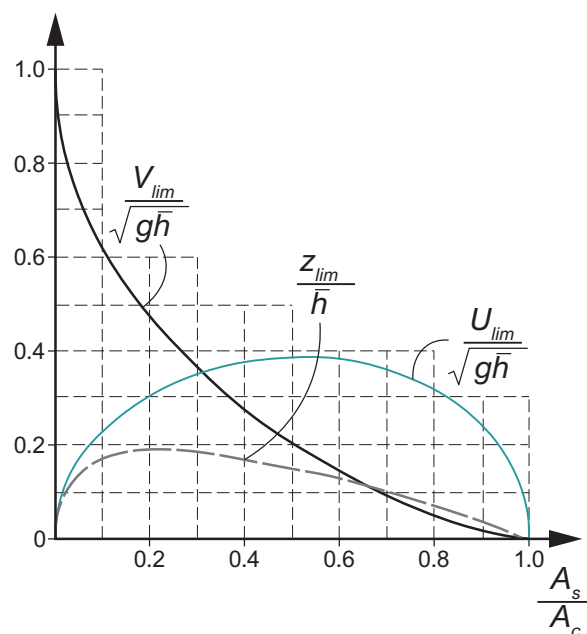


Figure 4.4: Limit values according to Schijf's theory (by TU Delft – Ports and Waterways is licenced under CC BY-NC-SA 4.0).

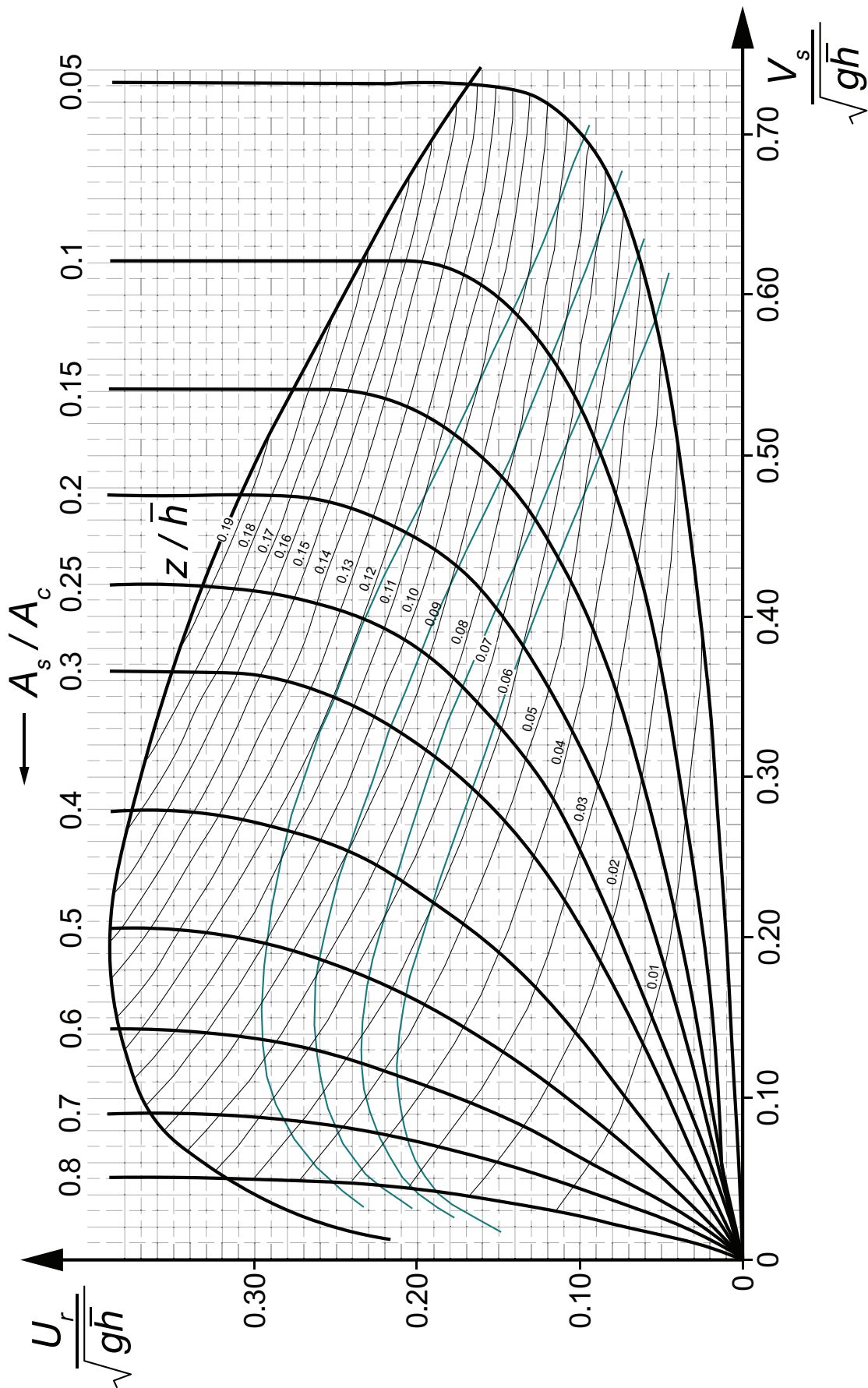


Figure 4.5: Schijf's diagram ( $\alpha_{Schijf} = 1.0$ ) (by TU Delft – Ports and Waterways is licenced under CC BY-NC-SA 4.0).

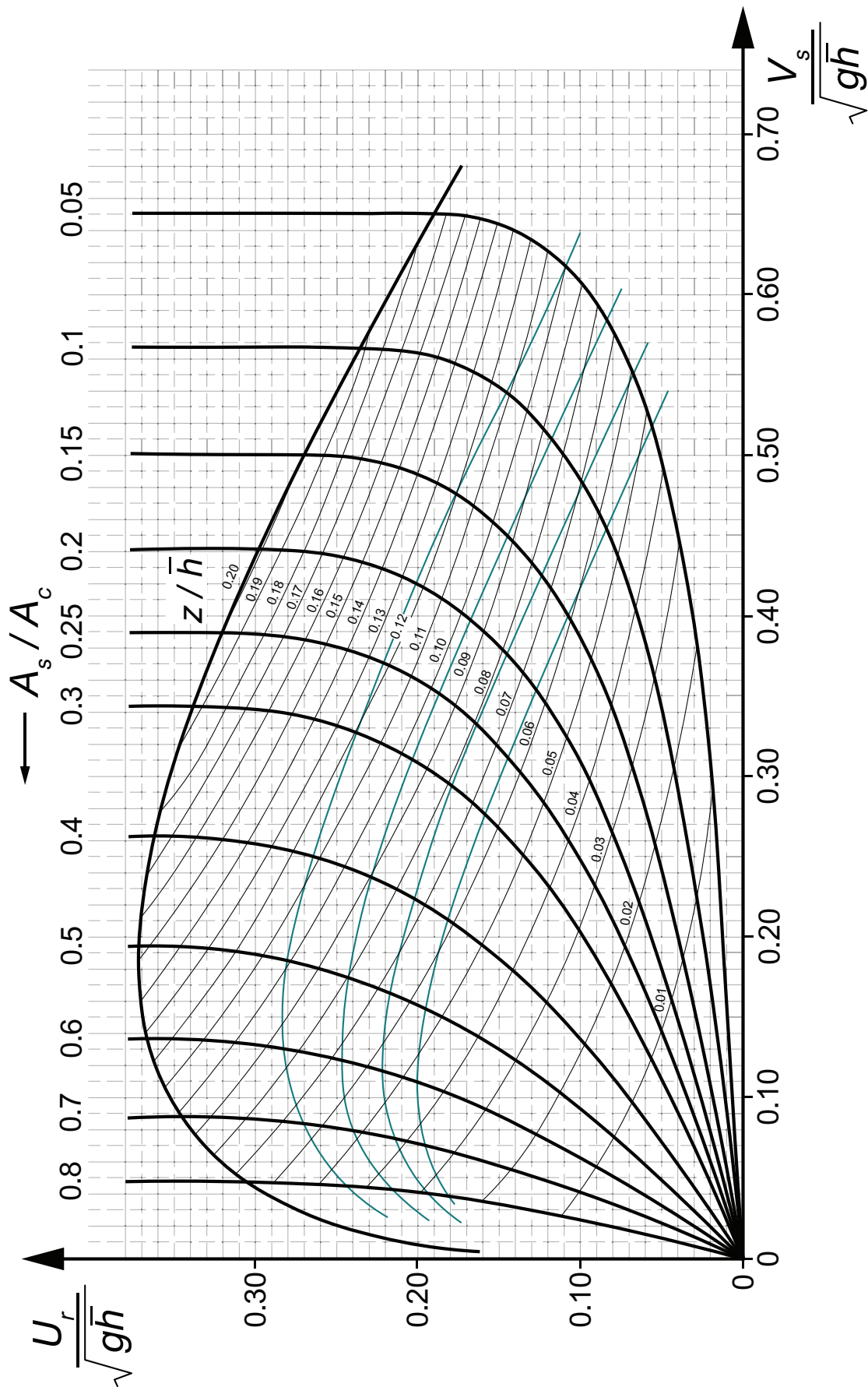


Figure 4.6: Schijf's diagram ( $\alpha_{Schijf} = 1.1$ ) (by TU Delft – Ports and Waterways is licenced under CC BY-NC-SA 4.0).



**Correction factor**

Tests (Delft Hydraulics, 1953) showed some deviations from this theory, probably due to the simplifying assumptions made. Therefore, a correction factor was introduced into Equation 4.1:

$$z = \alpha_{schijf} \frac{(V_s + U_r)^2}{2g} - \frac{V_s^2}{2g} \tag{4.13}$$

in which

$$\alpha_{schijf} = 1.4 - 0.4 \frac{V_s}{V_{lim}} \tag{4.14}$$

The correction factor generally varies between 1.05 and 1.2. A commonly used value is 1.1, which corresponds with  $V_s = 0.75V_{lim}$ . The effect of this correction is that the water level depression and the return current are larger than according to the original theory.

This factor is claimed to correct for the non-uniformity of the velocity field, but a comment is in order, because from a physical point of view it is not a very logical approach. Firstly, it is only applied in the expression for the energy head near the ship, not in the energy head away from the ship or in equation of continuity. Yet, applying the correction factor seems to improve the results, so it is usually maintained.

Taking this correction factor into account, the relationship between  $V_s$ ,  $U_r$  and  $z$  following from Equation 4.13 and Equation 4.2 reads (Equation 4.16 follows from Equation 4.2 in a similar manner as before):

$$\frac{V_s}{\sqrt{gh}} = \left( \frac{2 \frac{z}{h}}{\alpha_{schijf} \left( 1 - \frac{A_s}{A_c} - \frac{z}{h} \right)^{-2} - 1} \right)^{1/2} \tag{4.15}$$

$$\frac{U_r}{\sqrt{gh}} = \frac{V_s}{\sqrt{gh}} \left( \frac{1}{1 - \frac{A_s}{A_c} - \frac{z}{h}} - 1 \right) \tag{4.16}$$

Figure 4.5 and Figure 4.6 show diagrams of  $U_r/\sqrt{gh}$  as a function of  $V_s/\sqrt{gh}$  for different values of  $z/\bar{h}$ , with  $\alpha_{schijf} = 1.0$  and  $1.1$ , respectively. Moreover, the diagrams indicate what fraction of the limit speed each point concern. Given  $A_s/A_c$ ,  $g$ ,  $\bar{h}$  and  $V_s$ , one can determine  $U_r$ ,  $z$  and  $V_{lim}$ .

**Example box 4.1: Compute  $V_{lim}$ ,  $z_{lim}$ ,  $U_{lim}$  and  $U_r$**

Consider a rectangular channel similar to the Amsterdam-Rhine Canal:  $h_0 = \bar{h} = 5$  m and  $W_s = 100$  m. The largest push-tow convoy allowed to sail in the canal, a four-barge unit, has dimensions:  $L_s = 191$  m,  $B_s = 22.8$  m,  $D_s = 3.3$  m. The ship sails in the centreline of the canal. What are the limit conditions  $V_{lim}$ ,  $z_{lim}$  and  $U_{lim}$  and what are  $U_r$  and  $z$  if  $V_s = 3.5$  m/s?

The blockage coefficient  $A_s/A_c$  is a parameter that appears throughout the equations of Schijf's theory. In this case it amounts to:

$$A_s/A_c = B_s D_s / W_s h_0 = 22.8 * 3.3 / (100 * 5) = 0.15$$

The limit speed  $V_{lim}$  can be determined in different ways:

(a) iteratively from Equation 4.10, which is the most accurate approach:

$$\left( \frac{V_{lim}}{\sqrt{gh}} \right)^2 - 3 \left( \frac{V_{lim}}{\sqrt{gh}} \right)^{\frac{2}{3}} = -2 \left( 1 - \frac{A_s}{A_c} \right) = -1.70$$

Example box 4.1 – continued on next page

**Example box 4.1 – continued from previous page**

(b) if  $A_s/A_c$  lies between 0.1 and 0.3, Equation 4.10 can be approximated by

$$\frac{V_{lim}}{\sqrt{gh}} \approx 0.78 \left(1 - \frac{A_s}{A_c}\right)^{2.25} = 0.54$$

(c) by reading from Figure 4.5 (assuming  $\alpha_{Schijf} = 1.0$ ), yielding  $V_{lim}/\sqrt{gh} = 0.55$ .

The consensus result is  $V_{lim} = 3.79$  m/s.

The limit water level depression  $z_{lim}$  preferably follows from Equation 4.6:

$$z_{lim}/\bar{h} = 1/3(1 - 0.15 - 0.541^2) = 0.186$$

yielding  $z_{lim} = 0.93$  m. Reading from Figure 4.5 gives a (less accurate) value of 0.9 m.

The limit return current velocity  $U_{lim}$  follows from Equation 4.12:

$$U_{lim}/\sqrt{gh} = \sqrt{\frac{2}{3}(1 - 0.15) + \frac{1}{3}0.541^2} - 0.541 = 0.274$$

so  $U_{lim} = 1.91$  m/s. Reading from Figure 4.5 yields 1.89 m/s, but is less accurate.

The return current  $U_r$  when the convoy sails at 3.5 m/s can be found in two ways:

(a) iteratively from

$$((V_s + U_r)^2 - V_s^2)/(2g\bar{h}) - U_r/(V_s + U_r) + A_s/A_c = 0$$

which follows from elimination of  $z$  from Equation 4.1 and Equation 4.2. This yields  $U_r = 1.13$  m/s.

(b) by reading from Figure 4.5, yielding the (less accurate) value of 1.13 m/s.

The water level depression  $z$  follows either from Equation 4.13, yielding 0.47 m, or from Figure 4.5, yielding the same result.

**Non-rectangular cross-sections**

Schijf's model was originally developed for rectangular channels. A simple schematisation suffices to extend the method to trapezoidal channels and actually to any shape of cross-section, as long as it can be approximated

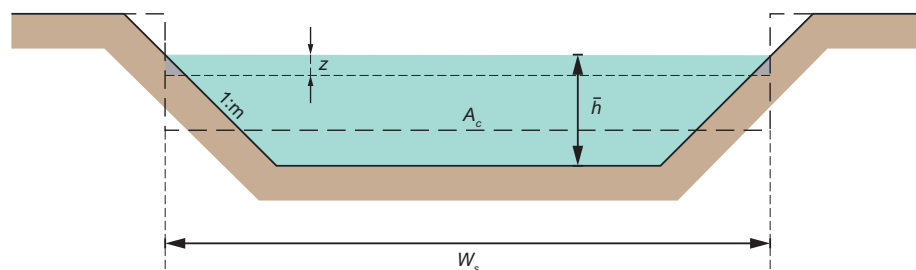


Figure 4.7: Schematisation of a trapezoidal cross-section (by TU Delft – Ports and Waterways is licenced under CC BY-NC-SA 4.0).

by a rectangle with the same wet cross-section and the same width at the water surface. Figure 4.7 shows this schematisation for a trapezoidal channel.

Schijf's method can be applied without modification to the schematised channel. The error due to this schematisation depends on the bank slope ( $1 : m$ ), the width at the water surface ( $W_s$ ) and the water level depression ( $z$ ). When a ship passes, there is a small error in the cross-sectional area (the grey areas in Figure 4.7), amounting to  $mz^2$  relative to  $A_c - A_s - W_s z$ .

If the blockage coefficient  $A_s/A_c$  is less than 0.1, the error due to the schematisation is less than 1 to 2%. For larger blockage coefficients this may increase to some 5%.

Balanin and Bykov (1965) present equations for the limit speed in a trapezoidal canal (Equation 4.17), as well as an iterative method to determine return current and water level depression (Equation 4.18 to Equation 4.20):

$$\frac{V_{lim}}{\sqrt{gh_0}} = \sqrt{8} \left( 1 - 0.325 \frac{mh_0}{W_s} \right) \left[ \cos \left( \frac{\pi + \arccos \left( 1 - \frac{A_s}{A_c} \right)}{3} \right) \right]^{\frac{3}{2}} \quad (4.17)$$

$$z = \frac{V_s^2}{g} \left( \frac{\frac{A_c}{A_s} - 0.5}{\left( \frac{A_c}{A_s} - 1 \right)^2} \right) \quad (4.18)$$

$$U_r = V_s \left( \frac{1 + z \frac{W_s}{A_s}}{\frac{A_c}{A_s} - 1 - z \frac{W_s}{A_s}} \right) \quad (4.19)$$

$$z = \frac{1}{g} (V_s + 0.5U_r)U_r \quad (4.20)$$

In a few iterations this method already yields reliable results.

In wide channels the blockage factor is small and the return current velocity is much smaller than the ship's speed. Bolt (2003) derived for the return current in that case:

$$U_r = V_s \left( \frac{\frac{A_s}{A_c}}{1 - \frac{A_s}{A_c} - Fr_h^2} \right) \quad (4.21)$$

in which  $Fr_h$  is again the Froude number related to the ship speed and the water depth.

### Natural waterways with a current

The computations for channels with a current are analogous to the ones for channels without currents. Only now the velocities have to be considered relative to the current velocity in the undisturbed channel.

Suppose:

- $U_c$  = undisturbed absolute current velocity (i.e. relative to the banks),
- $V_s$  = absolute speed of the ship,
- $V'_s$  = ship's speed relative to the undisturbed channel flow,
- $U_r$  = absolute return current velocity,
- $U'_r$  = return current velocity relative to the undisturbed channel flow.

Furthermore, we define in Figure 4.8 the direction from left to right as positive. Then the relative ship's speed to be used in the analysis is

$$V'_s = V_s - U_c \quad (4.22)$$

The method then yields the relative return current velocity  $U'_r$ , after which the absolute one follows from

$$U_r = U'_r - U_c \quad (4.23)$$

The easiest way of taking the current into account is therefore to work from a ship-fixed co-ordinate system. On board of the ship one sees the undisturbed water approach at a speed  $V'_s$  and next to the ship the flow has a speed  $V_s + U_r + / - U_c$ . Note that  $U_c$  can be positive or negative, which means that  $U_r$  may become negative. In that case, Schijf's method does not apply.

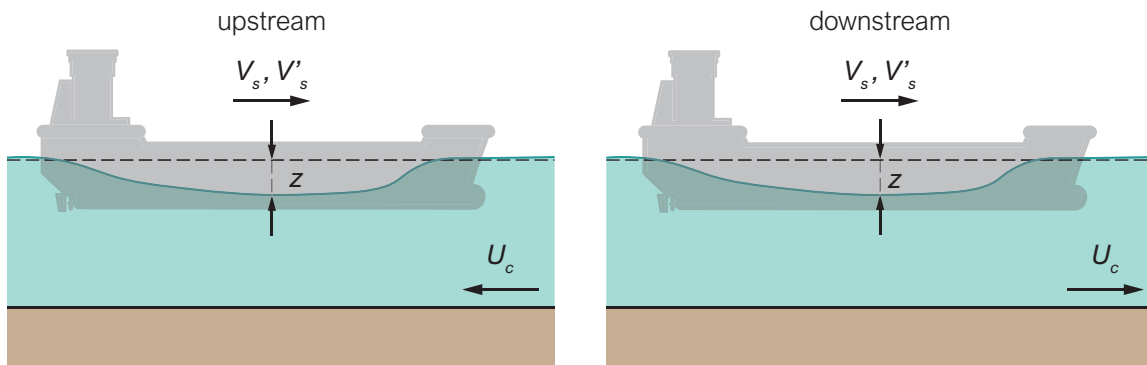


Figure 4.8: Waterway with a current (by TU Delft – Ports and Waterways is licenced under CC BY-NC-SA 4.0).

#### 4.1.2 Momentum conservation approach

Instead of considering the conservation of energy of the water motion, Bouwmeester et al. (1977) considered the momentum balance for the body of water before and around the ship (the grey area in Figure 4.9). The basis of this approach is Newton's law, i.e.

$$\sum F = M \frac{dV}{dt} \quad (4.24)$$

where  $\sum F$  is the sum of longitudinal forces on the water body around ship,  $M$  is the water mass considered,  $V$  is the velocity and  $t$  is time. Note that the time-derivative is a material derivative, i.e. moving along with the flow.

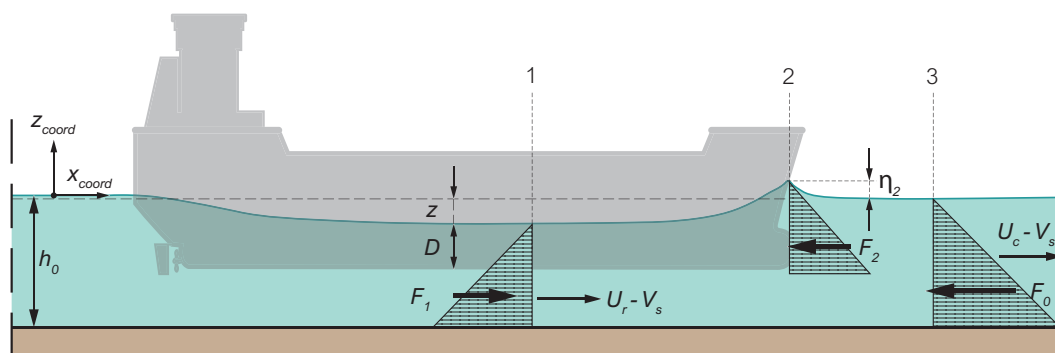


Figure 4.9: Control area of the momentum conservation approach (modified from Bouwmeester et al., 1977, by TU Delft – Ports and Waterways is licenced under CC BY-NC-SA 4.0).

In the case of steady horizontal frictionless water flow, this can be elaborated to

$$\frac{F_h}{\rho_w} + \frac{Q^2}{A} = \text{constant in the flow direction} \quad (4.25)$$

in which  $F_h$  is the hydrostatic force,  $\rho_w$  is the mass density of water,  $Q$  is the discharge and  $A$  is the cross-sectional area of the flow.

Because the basic conservation equations can be written in terms of energy conservation as well as momentum conservation, the results of these two approaches should be the same. Bouwmeester et al. (1977) derived their results for a trapezoidal channel, but even if they are translated to a rectangular channel, there are discrepancies, probably due to a difference in assumptions.

Sharp and Fenton (1968) developed a simplified model based on momentum conservation, assuming a rectangular cross-section ( $m = 0$ ) and neglecting the current velocity ( $U_c = 0$ ) and the headwater in front of the bow.

Computed values with Schijf's and Bouwmeester's approaches have been compared with measured data. In the case presented in Figure 4.10 both theories show a considerable degree of agreement in other cases larger discrepancies are found.

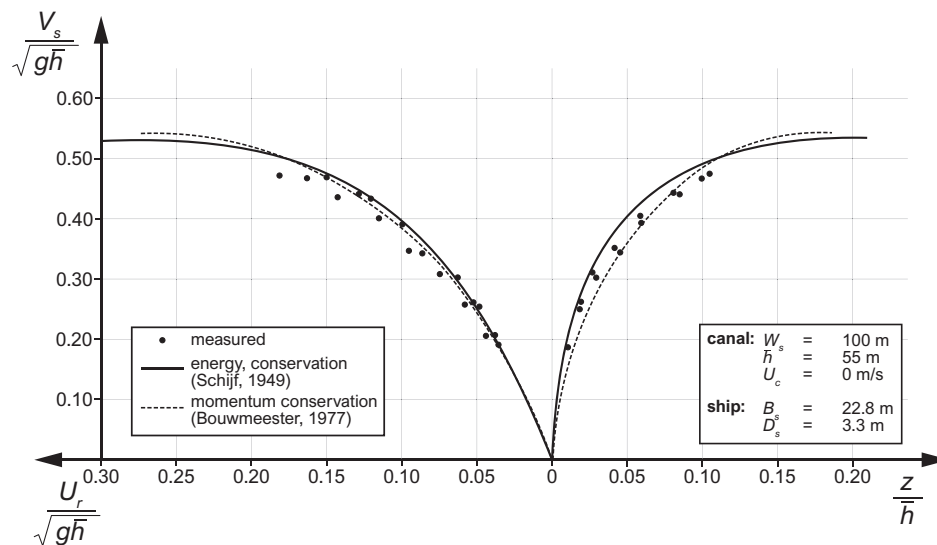


Figure 4.10: Comparison of computed and measured values for a push-tow unit (reworked from Bouwmeester et al., 1977, by TU Delft – Ports and Waterways is licenced under CC BY-NC-SA 4.0).

For the one-dimensional approach to be applicable, the channel width must not be much larger than the length of the ship ( $L_s$ ), otherwise the assumption of uniformity across the channel will no longer hold. The ratio  $W_s/L_s$  must certainly not be larger than 1.5. Considering the fact that for inland ships the length-beam ration is usually in the order of 8, the field of application for the one-dimensional model is  $2 < W_s/B_s < 12$ .

Experiments (Delft Hydraulics, 1985) showed that within these constraints Bouwmeester's momentum approach gives the best results for the water level depression and the return current velocity. For conventional ships the energy method of Schijf appeared to perform within the range  $2 < W_s/B_s < 4.5$ . The energy method also appeared to apply well for push-barge units in the same range.

In fact the application of one-dimensional models is only permitted for ships sailing in the centre line the canal (midway). Tests in the Hartel Canal (near Rotterdam) on the water motion caused by a pushed convoy revealed that the water level depression and the return current increase as the ship sails more eccentrically (Delft Hydraulics, 1984). For the governing equations we refer to Delft Hydraulics (1988) or the (CIRIA; CUR; CETMEF, 2007).

Note, furthermore, that in the considerations so far the influence of bed, bank and hull friction has not been taken into account, since it was assumed to be of minor importance. Including these friction effects turned out to yield only 3% extra water level depression. This only applies in case of a substantial under keel clearance, otherwise the boundary layers along the ship's hull and at the canal bed will interfere.

## 4.2 Secondary water motion

Besides the primary wave system, sailing ships generate so-called secondary waves (though these are probably the most visible ones). At a normal sailing speed these waves remain short with respect to the ship's length. Below a relative speed of  $0.233 \text{ m/s}$  they tend to be suppressed by the surface tension. As the speed increases beyond this value, first small capillary waves (wave length  $< 1.7 \text{ cm}$ ) will be generated, but at still higher speeds longer gravity waves will form. These are important for navigation, but also for safety, e.g. of moored other vessels, or of people at the banks.

The theoretical basis explaining ship-induced waves was laid by Lord Kelvin (Kelvin, 1886, 1887, 1904). In his theory, he first considered a ship sailing at a constant speed as an isolated pressure point, moving over the surface of deep water while transmitting a wave pattern. Observations and theoretical investigations show that for a moving ship two groups of waves are created: one near the bow and the other in the stern region of the ship. Moreover, each of these groups consists of two systems of waves, the so-called divergent and transversal waves. The former diverge away from the axis of navigation, the latter propagate in the direction of navigation, but at a speed that decreases with the distance to the axis (Figure 4.11).

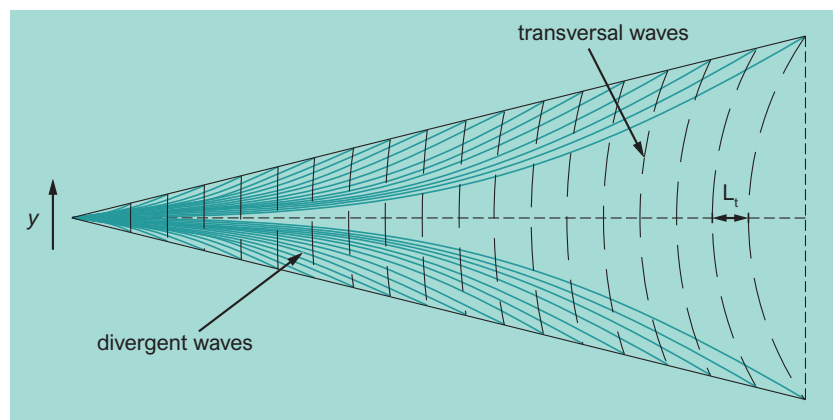


Figure 4.11: Waves according to Kelvin's moving pressure point theory (by TU Delft – Ports and Waterways is licenced under CC BY-NC-SA 4.0).

At the locations where the divergent and the transversal waves meet, so-called interference cusps are formed. Cusps occur at points where two or more waves arrive simultaneously. The height of the cusp is determined by the sum of the heights of the individual incoming waves. At deep water and for an isolated pressure point these cusps are located on a line at an angle of  $19^\circ 28'$  ( $\sin 19^\circ 28' = 1/3$ ) with respect to the sailing line (Figure 4.12).

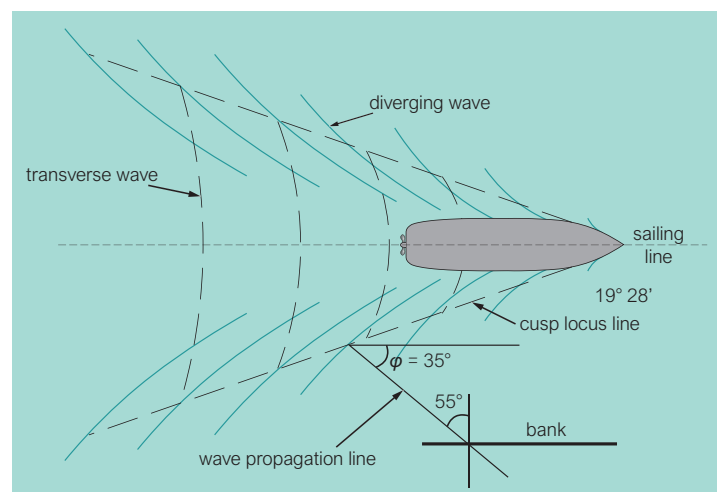


Figure 4.12: Locus of interference cusps (by TU Delft – Ports and Waterways is licenced under CC BY-NC-SA 4.0).

**Deep water** A ship sailing on deep water can be seen as an assembly of a large amount of pressure points: mainly at the bow and at the stern, but also with interruptions along the water line, for example at the location between two inland barges. This causes a wave pattern around a sailing ship as shown in [Figure 4.12](#) (only the bow system is shown).

Two systems of interference cusps are induced, viz. one at the bow and one at the stern of the ship. From observations the angle  $\theta$  between the cusp lines and the sailing line appears to be a little smaller than the aforementioned  $19^\circ 28'$ , and varies between  $10^\circ$  and  $19^\circ 28'$ , depending on the shape of the ship. The transversal waves are usually only clearly noticeable behind the ship, since no disturbances occur outside the cusp lines from the bow.

In the navigation axis the position of the transversal wave crests with respect to the bow is given by

$$x_n = n \frac{2\pi}{g} V_p^2 = nL_t \quad (4.26)$$

where:

- $n$  = 1, 2, 3, ... = the number of the n-th wave crest from the bow,
- $V_p$  = the (absolute) celerity of the wave crest,
- $L_t$  = the distance between two successive wave crests (so the wave length).

The relation between the length of the ship-induced transversal waves and the navigation speed can be determined through linear wave theory. According to this theory, for gravity waves at deep water the wave length  $\lambda$  and the wave celerity  $c$  are related via the dispersion relationship:

$$c^2 = \frac{g}{2\pi} \lambda \quad (4.27)$$

The sailing speed can be considered as the celerity of a certain point that induces waves. If we assume  $V_p = V_s$ , [Equation 4.27](#) implies

$$L_t = \frac{2\pi}{g} V_s^2 \quad (4.28)$$

This equation reveals another natural limit velocity. If a small ship with large engine power increases its speed more and more, the wave length of the transversal wave will approach the ship's length  $L_s$ . In that case bow wave and stern wave interfere and reinforce each other to maximum amplitude. If the ship would further increase its speed, it ship would have to sail against its own bow wave, which at the same time becomes higher. As a consequence, applying more engine power does not further increase the ship's speed. Only ships with a special design can overcome this by skimming over the water. For a normal ship the limit speed follows from:

$$V_{lim} = \sqrt{\frac{g}{2\pi} L_s} \quad (4.29)$$

**Shallow water** From a wave perspective, waves 'feel' the bed in shallow water, which is the case if  $h_0/\lambda < 0.5$ . The celerity of the individual waves is now described with the dispersion relationship

$$c^2 = gk \tanh(kh_0) \quad (4.30)$$

In case of the limit speed as defined above, the corresponding shallow-water wave length is equal to the ship length, again. If we assume the wave celerity to be equal to the ship speed, we have:

$$\frac{V_{lim, shallow}}{V_{lim, deep}} = \sqrt{\tanh\left(\frac{2\pi h_0}{L_s}\right)} = \sqrt{\tanh\left(\frac{gh_0}{V_{lim, deep}^2}\right)} \quad (4.31)$$

The Froude-number criterion can be used to distinguish between deep and shallow water conditions for the ship: if  $Fr_h = V_s/\sqrt{gh_0} < 0.74$ , the ship experiences deep water conditions.

The angle  $\theta$  also depends on this ship-based Froude number. For  $Fr_h$ -values up to 0.74, the angle differs little from the  $19^\circ 28'$  for deep water. For values larger than 0.74 a rapid increase of the angle occurs, up to  $90^\circ$  when the critical velocity is reached ( $Fr_h = 1$ ), Figure 4.13. At that moment the transversal and divergent waves will coincide and create a kind of shock wave, similar to the sound barrier for flying objects at Mach 1. When the ship's speed increases further, the transversal waves disappear and only divergent waves remain. At a still higher speed, the angle  $\theta$  will gradually decrease back to  $19^\circ 28'$ . This situation, however, is not relevant for water-displacing ships, only for planing vessels such as fast ferries, see Section 4.2.4.

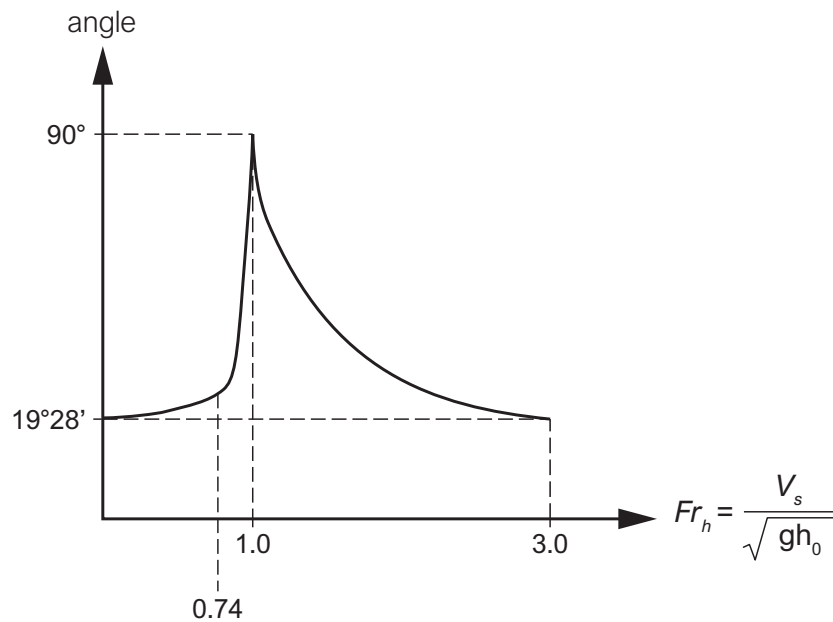


Figure 4.13: Angle  $\theta$  as a function of the Froude number (by TU Delft – Ports and Waterways is licenced under CC BY-NC-SA 4.0).

In case of a limited channel width, reflection at the banks plays a role. It leads to extra interferences, depending on the reflection properties of the banks, the ship's speed, the ratio of the channel width and the ship length, and whether the ship sails in the centreline or eccentrically.

Furthermore, the secondary water motion is strongly influenced by the strength of the primary motion. Generally speaking, the influence of the ship-induced waves will decrease as the return current and the water-level depression increase. This means that small fast ships are responsible for most of the wave attack on the banks, whereas large slow ships cause most of the current attack.

#### 4.2.1 Wave height of interference cusps

An empirical relation based on scale model tests (Verheij and Bogaerts, 1989) for the maximum height of the interference cusps cause by ships sailing at a moderate speed ( $Fr_s < 0.8$ ) in relatively deep open water:

$$H_i = 1.2\alpha_i h_0 \left(\frac{y_s}{h_0}\right)^{-0.33} Fr_h^4 \quad (4.32)$$

for  $h_0/L_{wi} > 0.25$ ,  $H_i/L_{wi} < 0.14$  and  $H_i/h_0 < 0.6$ .



Where:

- $H_i$  = height of interference cusps,
- $y_s$  = distance to the side of the ship,
- $\alpha_i$  = coefficient between 0.85 and 1.00, depending on the type and shape of the ship,
- $L_{wi}$  = wave length of the interfering waves.

The conditions in Equation 4.32 imply deep-water wave propagation and non-breaking waves.

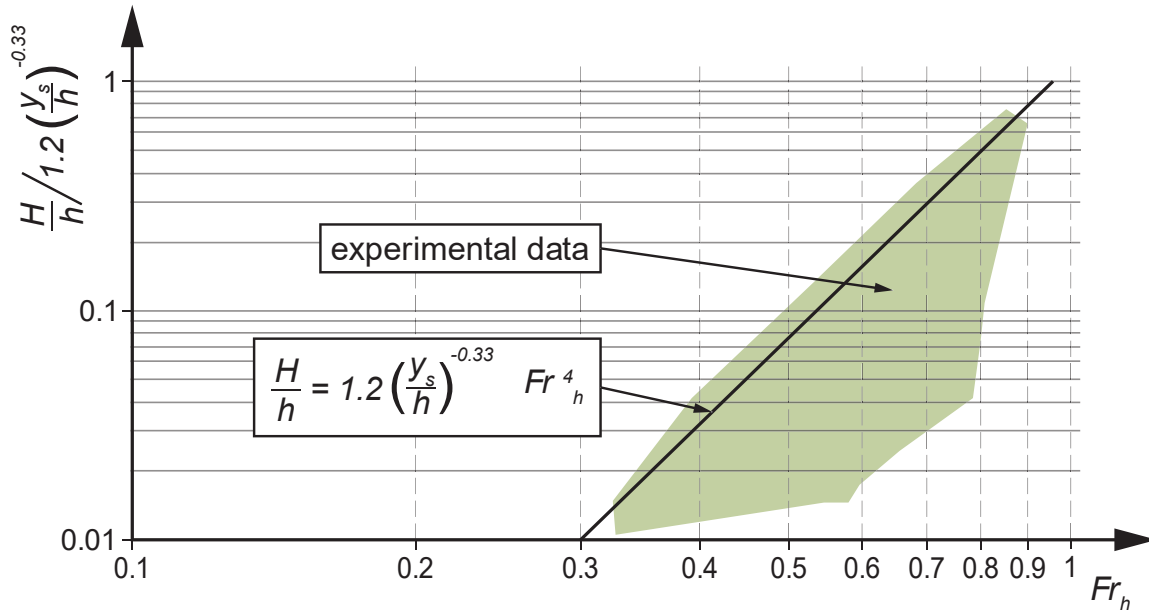


Figure 4.14: Occurring heights of interference cusps (by TU Delft – Ports and Waterways is licenced under CC BY-NC-SA 4.0).

Numerical modelling is recommendable to determine the height of ship-induced waves (e.g. Doorn et al., 2002); also see Section 4.6.

#### 4.2.2 Wave height of transversal waves

The height of the transversal waves around the sailing axis can be described with a similar empirical relationship, but now the relevant distance is the one between the wave crest and the ship's stern:

$$H_t = 4.0h_0 \left( \frac{x_t}{h_0} \right)^{-0.5} Fr_h^4 \quad (4.33)$$

for  $h_0/L_t > 0.25$ ,  $H_t/L_t < 0.14$  and  $H_t/h_0 < 0.6$ .

where:

- $H_t$  = height of transversal waves
- $x_t$  = distance behind the ship
- $L_t$  = wavelength of the transversal waves.

Tests have demonstrated that a relation exists between the wave height  $H_t$  and the ship's speed, namely:

$$H_t = \gamma_t \cdot \frac{V_s^2}{g} \quad (4.34)$$

Figure 4.15 visualises this relation. The value of  $\gamma_t$  varies between 0.085 and 0.170 with an average value of 0.154.

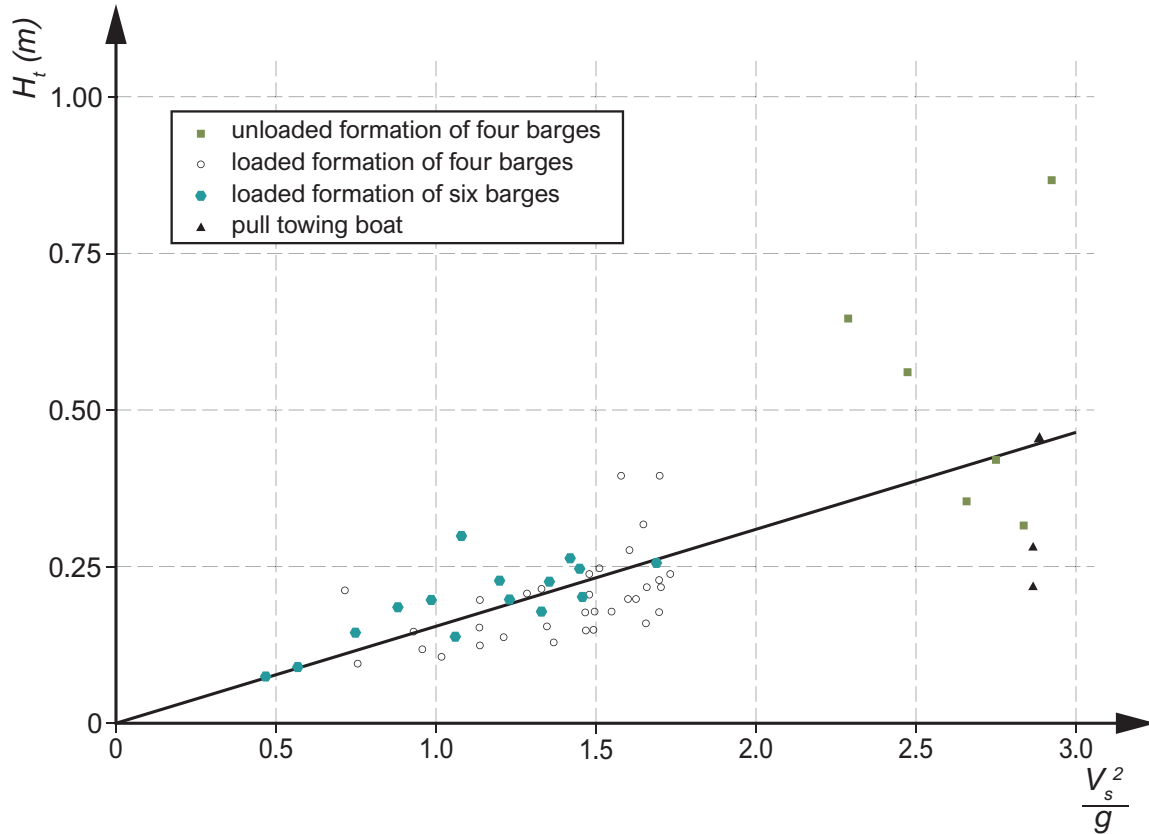


Figure 4.15: Height of transversal waves (by TU Delft – Ports and Waterways is licenced under CC BY-NC-SA 4.0).

### 4.2.3 Wave length of the divergent waves

The wave length of the transversal waves on deep water follows from Equation 4.28. The divergent waves are propagating under an angle  $\phi$  with the navigation direction (Figure 4.13). The propagation speed of these waves is therefore  $V_s \cos \phi$  and the deep-water wave length follows from:

$$L_d = \frac{2\pi}{g} V_s^2 \cos^2 \phi \quad (4.35)$$

The propagation speed of the cusps is also equal to  $V_s \cos \phi$ , so the distance between consecutive cusps is equal to the wave length of the divergent waves. The direction of propagation of the cusps is perpendicular to the cusp line, so in deep water under an angle of  $(90^\circ - 19^\circ 28')/2 = 35^\circ 16'$  with the navigation direction of the ship. Since  $\cos 35^\circ 16' = 0.82$ , the distance between two consecutive cusps becomes:

$$L_{wi} = 4.2 h_0 Fr_h^2 \quad (4.36)$$

and the propagation speed of the cusp is  $0.82 V_s$ . The return period of the cusps at a fixed point is

$$T_{wi} = 5.1 h_0 Fr_h \quad (4.37)$$

### 4.2.4 Fast ferries

The wave pattern changes for Froude numbers greater than 0.85, as the hydrodynamic conditions change from sub-critical via critical to super-critical. Figure 4.16 through Figure 4.18 show examples of this transition.

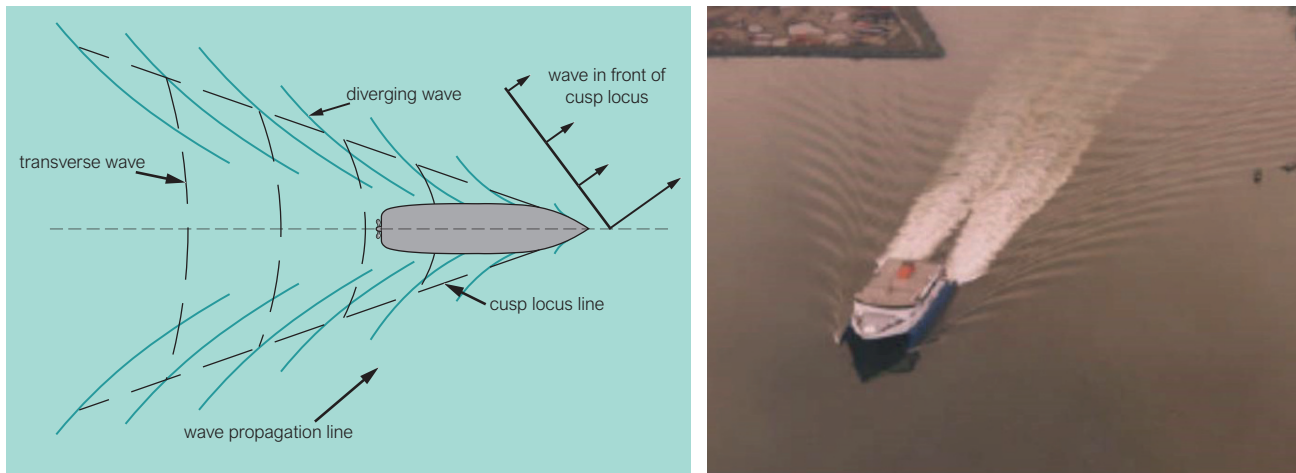


Figure 4.16: Planview and aerial photograph of catamaran with sub-critical wave pattern (by TU Delft – Ports and Waterways is licenced under CC BY-NC-SA 4.0).

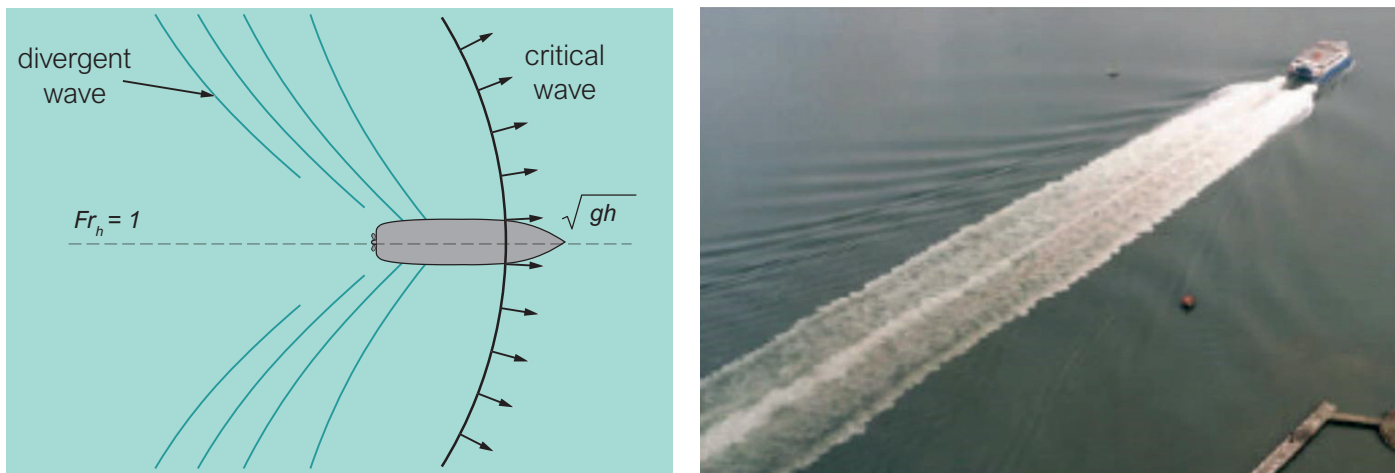


Figure 4.17: Planview and aerial photograph of catamaran passing critical conditions (by TU Delft – Ports and Waterways is licenced under CC BY-NC-SA 4.0).

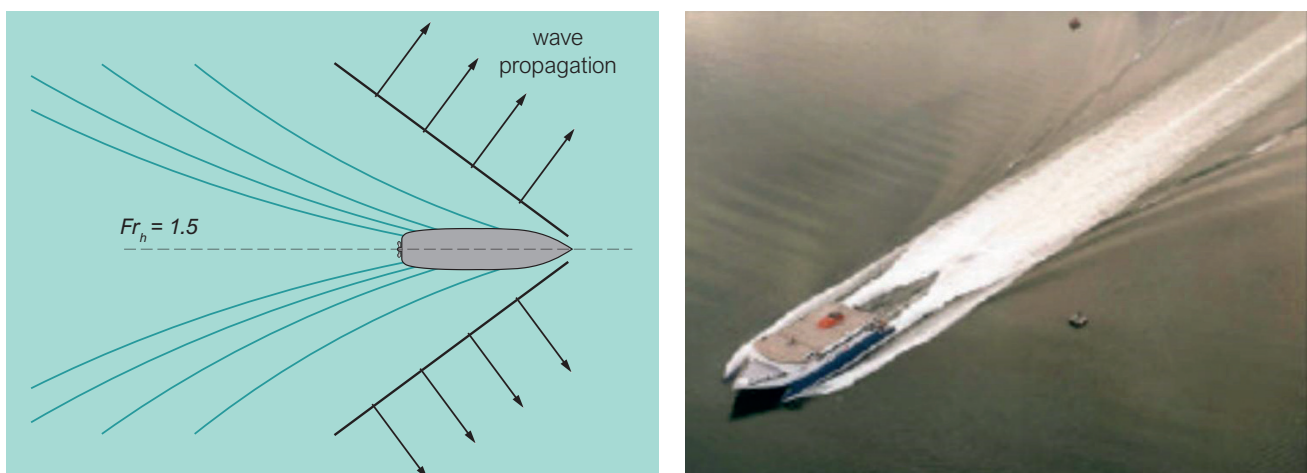


Figure 4.18: Planview and aerial photograph of catamaran with super-critical wave pattern (by TU Delft – Ports and Waterways is licenced under CC BY-NC-SA 4.0).

The waves caused by these fast ferries may cause hindrance to moored vessels and other sailing vessels. Figure 4.19 shows that the highest waves are generated at  $Fr_h$ -values around 1, when conditions change from subcritical to supercritical. Then wave resistance is maximal, and so are the generated waves.

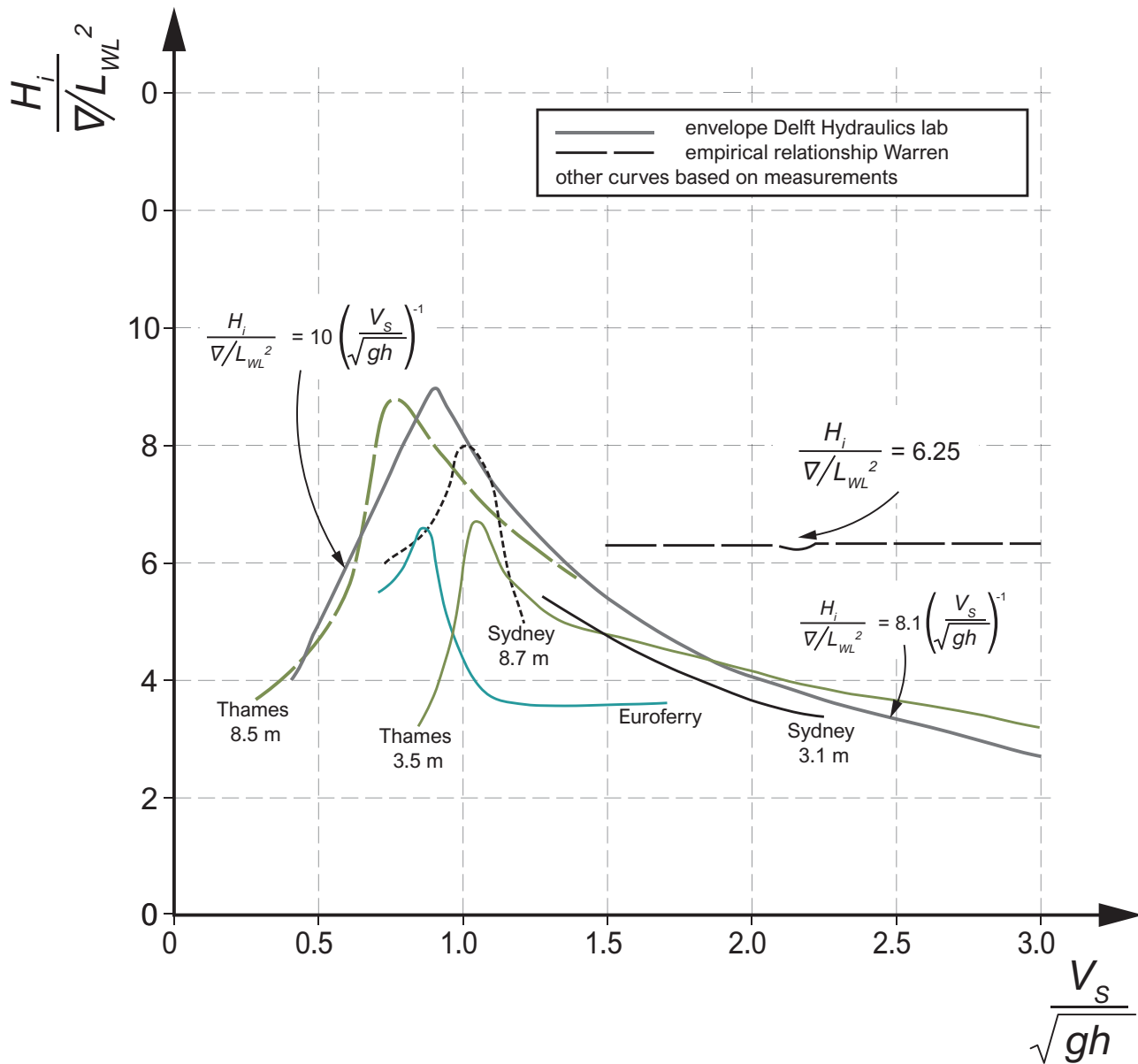


Figure 4.19: Measured wave heights of fast ferries (by TU Delft – Ports and Waterways is licenced under CC BY-NC-SA 4.0).

From literature study on waves generated by fast ferries, Delft Hydraulics (1994, 1998) found the following equations for the wave height:

$$Fr_h \leq 0.9 : H_i = 10 \frac{\nabla}{L_{WL}^2} Fr_h \quad (4.38)$$

$$Fr_h \geq 0.9 : H_i = 8.1 \frac{\nabla}{L_{WL}^2} Fr_h^{-1} \quad (4.39)$$

with  $Fr_h = \frac{V_s}{\sqrt{gh_0}}$  and

$L_{WL}$  = length of a ship on the water line (m)  
 $\nabla$  = water displacement ( $m^3$ )

The maximum wave height occurs for  $Fr_L = 0.4$  (or  $Fr_h$  about 1.0) with  $Fr_L = \frac{V_s}{\sqrt{gL_{WL}}}$ :

$$H_i = (7.75 \pm 1.25) \frac{\nabla}{L_{WL}^2} \quad (4.40)$$

The characteristic wave periods of super critical waves are 8 to 9 seconds.

### 4.3 Propeller and thruster jets

As ships become larger, the transport network needs to be adapted. Harbour basins have to be deepened, quay walls lengthened, approach channels and other waterways widened and deepened. Moreover, the increased engine power leads to problems with bottom protection in harbours and at berths. The induced jets cause higher flow velocities and thus larger forces on existing bottom protections, if any. PIANC report 180 (PIANC, 2015) provides detailed information on how to deal with flow velocities, required bed protection or scour depth.

An additional development aggravating this problem is that many modern ships not only have main propellers at the rear of the ship, but also bow and stern thrusters perpendicular to the vessel's axis. These facilities allow the ship to manoeuvre without the help of a tugboat. They are used especially for manoeuvres such as berthing and de-berthing. The main propeller at the rear predominantly produces a forward thrust, but can help manoeuvring by changing the direction of the rudders. Figure 4.20 shows a diagram of a cross section of the bow of a sea-going ship with a side view of a bow thruster and an indication of the velocities in the jet it produces.

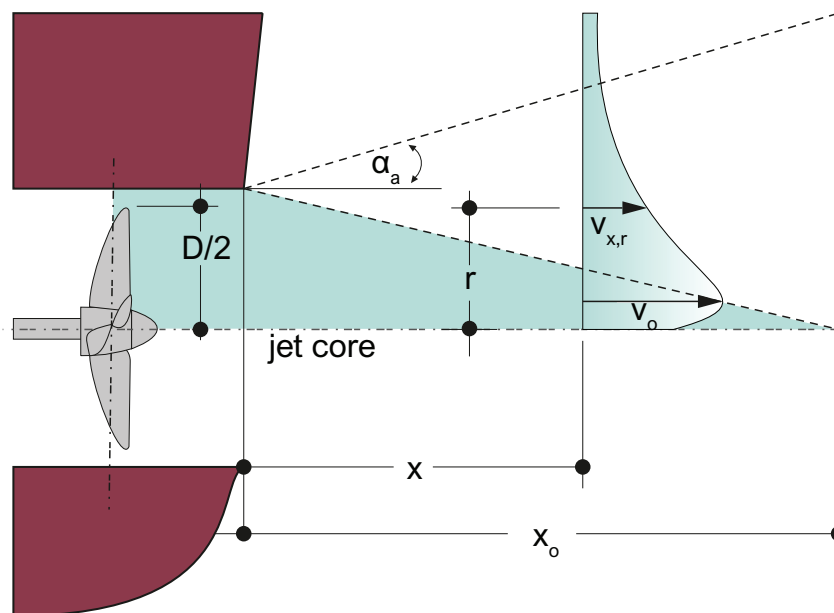


Figure 4.20: Bow thruster jet (by TU Delft – Ports and Waterways is licenced under CC BY-NC-SA 4.0).

The force produced by the bow thruster, combined with its distance to the centre of gravity of the ship, results in a large moment of forces that causes the front of the ship to turn away from the quay, for instance. After this, the main propellers are used for forward thrust in order to sail away. The increased size and power of thrusters and propellers causes jet velocities for which the bottom of the berth and the harbour basin have not been designed (Figure 4.21). This can lead to damage and failure of the bottom protection and severe bed erosion, with quay wall failure as a possible consequence.

Inland vessels are equipped with much smaller propulsion systems. Size and power vary widely and depend on the type of vessel and the navigation conditions, e.g. width and depth of the waterway and the presence of hydraulic structures such as locks. Ship types to be distinguished are: conventional cargo vessels, container vessels, push-tow units, passenger ships, recreational boats and service boats such as tugs and patrol vessels.

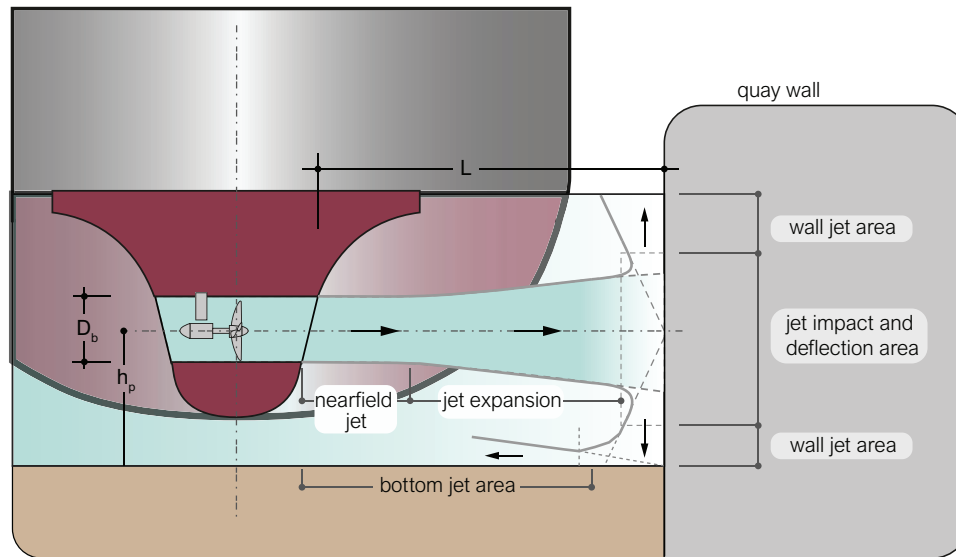


Figure 4.21: Thruster jet in the vicinity of a quay wall (by TU Delft – Ports and Waterways is licenced under CC BY-NC-SA 4.0).

In principle, all computation methods are based on the assumption that the propeller jet can be schematized as a submerged free jet discharging out of an orifice into an infinite fluid, and use the relevant equations for the zone of established flow presented by Albertson et al. (1950):

$$V_{axis} = \frac{V_0 D_p}{2Cx} \quad (4.41)$$

$$V_{x,r} = V_{axis} \exp \left[ -\frac{r^2}{2C^2 x^2} \right] \quad (4.42)$$

where:

$V_{axis}$	= flow velocity in the axis of the jet [m/s],
$V_0$	= efflux velocity [m/s]
$V_{x,r}$	= flow velocity in the jet at location $x, r$ [m/s]
$D_p$	= diameter of a free jet or propeller [m]
$x$	= horizontal distance from the propeller [m]
$r$	= radial distance from the jet axis [m]
$C$	= coefficient [-]

Albertson et al. (1950) determined a value of 0.081 for the coefficient  $C$ . Equation 4.42 describes a distribution of the flow velocity around the jet axis and applies to the zone of established flow. Closer to the orifice, in the nearfield zone, the flow has not yet established and different formulae should be used.

Note that a propeller jet differs at certain points from a free jet, e.g.

- higher turbulence levels due to propeller-induced rotation and whirl,
- reduced velocities in the centre of the jet core, due to the presence of the shaft, and
- shorter zone of flow establishment.

## Outflow velocity

Blaauw and Van de Kaa (1978) present the following equation for the outflow velocity, known from maritime engineering:

$$V_0 = C_3 \left( \frac{f_p P_s}{\rho_w D_p^2} \right)^{0.33} \quad (4.43)$$

where:

- $P_s$  = maximum installed engine power [W],
- $f_p$  = percentage of installed engine power [-], and
- $D_p$  = the propeller diameter [m].

Based on information of pilots and skippers (PIANC, 2015), the following values are recommended for  $f_p$ :

- thruster:  $f_p = 1.0$ , because always 100% of the installed power will be applied;
- main propellers:  $f_p = 0.05$  to  $0.15$ , but values up to  $0.40$  cannot be excluded.

Typical values for the coefficient  $C_3$  are  $1.17$  for ducted propellers and  $1.48$  for free propellers, but other values are mentioned in literature.

When substituting for a free (i.e. non-ducted) propeller a value of  $C_3 = 1.48$  and taking  $D_p = 1.41 \cdot D_0$ , with  $D_0$  the effective jet diameter, the coefficient of proportionality for a free propeller becomes  $1.17$ . As this is the same as for a ducted propeller with  $C_3 = 1.17$  and  $D_p = D_0$ , Blaauw and Van de Kaa (1978) presented one equation for both types of propellers:

$$V_0 = 1.15 \left( \frac{f_p P_s}{\rho_w D_0^2} \right)^{0.33} \quad (4.44)$$

In practice we only know  $D_p$ , so calculations have to be made with that quantity, irrespective of its uncertainty. If even  $D_p$  is unknown, the propeller diameter can be estimated by  $D_p = 0.6$  to  $0.7 D_s$ , where  $D_s$  is the ship's draught. The main propeller diameter of inland vessels is mostly  $1.8$  m and the bow thruster diameter  $0.8$  m.

On the basis of an inventory of the engine power installed in inland vessels, Verheij (2010) found the following relationships between the average installed main propeller power and the wet surface area of the hull:

$$P_{main} = 0.66 L_s (B_s + 2D_s) \quad (4.45)$$

In 90% in inland vessels, the installed power is less than about  $1.25 P_{main}$ . Outflow velocities of  $6$  to  $8$  m/s are normal.

## Flow distribution within the jet

To determine the velocity distribution in a jet, there are basically two approaches, a German and a Dutch one. For the German approach we refer to the PIANC WG 180 manual (PIANC, 2015). The Dutch approach is based on research by Blaauw and Van de Kaa (1978) and Verheij (1983). They found a value of the constant  $C$  of  $0.18$ , which is much larger than the value of  $0.081$  found by Albertson et al. (1950). This higher value corresponds with a faster spreading of the jet.

Substitution in Equation 4.41 and Equation 4.42 yields for the flow velocity in the jet axis:

$$V_{axis} = 2.8 \frac{V_0 D_p}{x} \quad (4.46)$$

and for the velocity profile perpendicular to the axis:

$$V_{x,r} = V_{axis} \exp \left[ -15.4 \frac{r^2}{x^2} \right] \quad (4.47)$$

In unconfined shallow water, the flow velocity at the bed follows from these two equations and the distance  $h_p$  of the propeller axis from the bed. Given the Gaussian character of  $V_{x,r}$ , the flow velocity distribution at the bed is likely to be Gaussian, as well, with the maximum below the propeller axis.

Test results largely agree on where the maximum flow velocity at the bed occurs (Verheij (1983):  $x/h_p = 4.5 \div 8$ ; Rajaratnam (1976):  $x/h_p = 4 \div 10$ ). If we assume  $x/h_p = 6$ , Equation 4.46 yields:

$$V_{b,max} = 0.3 \frac{V_0 D_p}{h_p} \quad (4.48)$$

### Multiple jets

In the case of two propellers and a limited UKC, the distance  $y_p$  between the propellers and the distance  $h_p$  from each propeller axis to the bed determine the velocity at the bed. According to Verheij (1983), superposition of jets is allowed in the cases considered here. Blokland (1997), however, derived for two propellers:

$$V_{max} = V_{single} \quad h_p/y_p < 0.578 \quad (4.49)$$

$$V_{max} = 0.43 \text{ to } 0.61 V_{single} D_0/r \quad 0.578 < h_p/y_p < 1 \quad (4.50)$$

$$V_{max} = V_{single} \sqrt{2} \quad h_p/y_p > 1 \quad (4.51)$$

with  $r = \sqrt{h_p^2 + y_p^2}$

### Other propulsion systems

In addition to the well-known main propellers, other propulsion systems are used in inland navigation. Examples are water jets, mainly applied in ferries and rescue vessels, and Voith Schneider (cycloidal drive) propellers, mainly used in tugs and ferries. We will discuss water jets in more detail here, because this type of propulsion can generate outflow velocities up to 25 m/s if the full engine power is applied. Hardly any bed protection can withstand such high flow velocities.

**Water jet propulsion** The axial pump driving the jet is more efficient than a propeller, and therefore produces higher speeds with the same energy expenditure and less vibration and noise. The jets are usually installed in pairs. Manoeuvring is possible by differential power application or by turning one of the jets forward (Figure 4.22). Maximum power can amount to 26 MW for sea-going ferries, yielding outflow velocities up to 25 m/s, whereas conventional propellers reach at most 8 – 10 m/s.

Verheij and Stolker (2007) derived the following set of formulae for the Kamewa water jet:

$$V_0 = 0.92 \left[ \frac{f_p P_s}{\rho_w A_0} \right]^{0.33} \quad (4.52)$$

$$V_{axis} = 12.4 V_0 x^{-1.17} \quad (4.53)$$

$$V_{x,r} = V_{max} \exp \left[ -92.75 \frac{r^2}{x^2} \right] \quad (4.54)$$



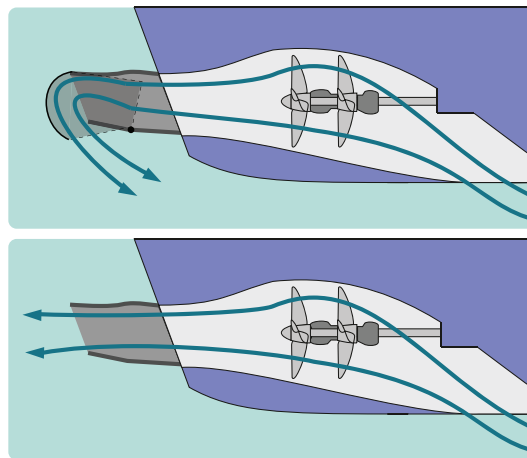


Figure 4.22: Water jet propulsion (reworked from: [Wikimedia Commons](#), by TU Delft – Ports and Waterways is licenced under CC BY-NC-SA 4.0)

in which  $A_0$  is the cross-sectional area of the outflow opening. The square opening of Kamewa jets is  $1 \text{ m}^2$ . If the outflow opening differs not much larger or smaller than  $1 \text{ m}^2$ , it can be translated into an equivalent circular opening with diameter  $D_{eq}$ . In that case Equation 4.53 can be replaced by:

$$V_{axis} = 10.8V_0 \left( \frac{D_{eq}}{x} \right)^{1.17} \quad (4.55)$$

Particularly dangerous for the stability of mobile beds is the possibility to direct these jets downwards. Kamewa jets can reach an angle of about 45 degrees (Figure 4.23), but other catamarans are equipped with jets that can be directed vertically.

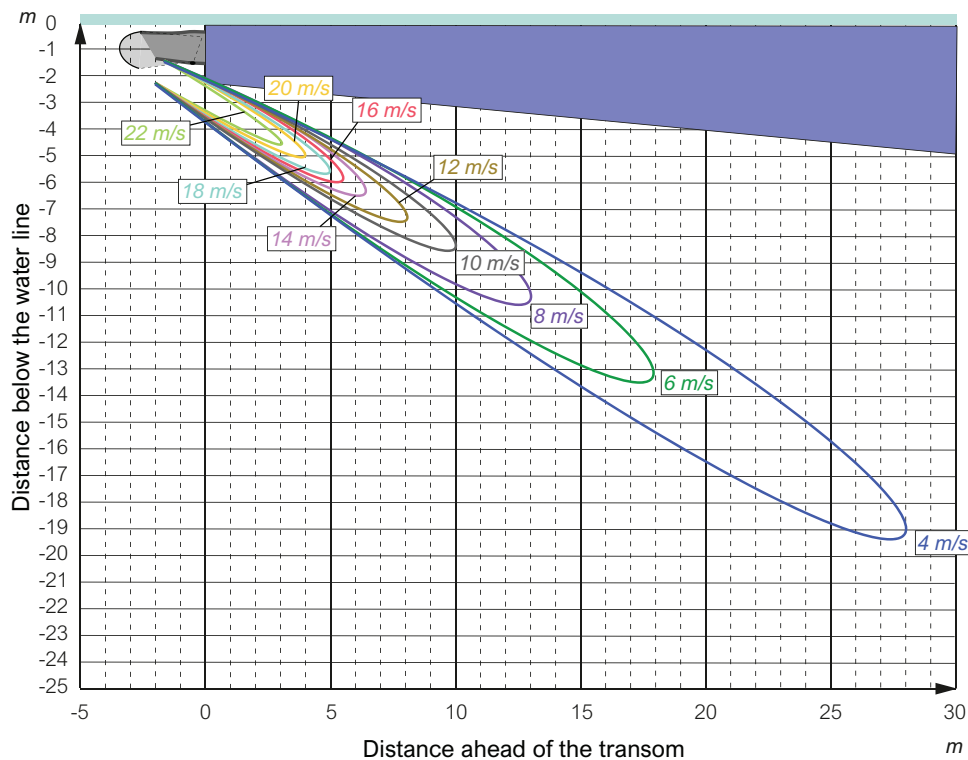


Figure 4.23: Flow velocities in a downward-directed Kamewa water jet (by TU Delft – Ports and Waterways is licenced under CC BY-NC-SA 4.0).

## 4.4 Other phenomena related to sailing ships

### 4.4.1 Stern waves

The primary water motion is described as consisting of a return current around the ship and a related water-level depression over the width of the waterway. The transition between the undisturbed water level in front of the vessel and the water-level depression beside the ship is called the front wave and the transition at the stern, between the water level depression and the undisturbed water level behind the vessel is called the stern wave. Both waves take the form of a sloping water surface (Figure 4.24).

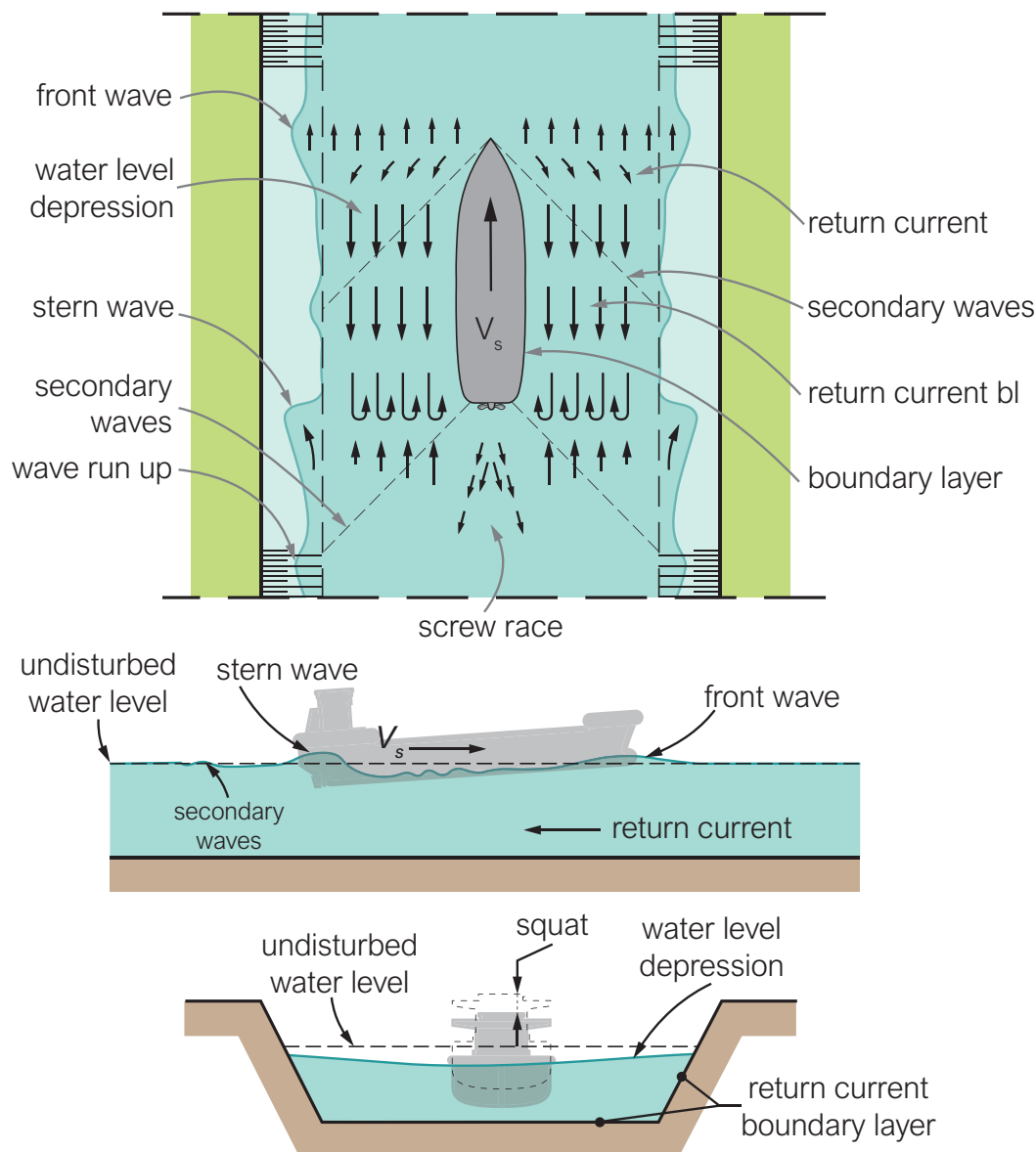


Figure 4.24: Ship-induced water motion (by TU Delft – Ports and Waterways is licenced under CC BY-NC-SA 4.0).

The height of the front wave is slightly greater than the water-level depression. The stern wave is the transition between the water-level depression and the normal water level behind the ship. This area is locally influenced by the water level depression associated with the propeller jet.

Both the front wave and the stern wave cause current velocities ahead of and directly behind the ship. The direction of these currents is the same as the navigation direction of the ship itself. The stern wave causes an attack at the bank slope protection which can be the determining factor for stability, especially for trapezoidal profiles. It becomes stronger as the ship sails closer to the bank.

The maximum water level elevation  $z_{max}$ , the water level gradient  $i_{max}$  and the maximum velocity  $u_{max}$  due to the stern wave follow from (Delft Hydraulics, 1988):

$$z_{max} = (1.5 \div 2.0)z \quad (4.56)$$

$$i_{max} \leq 0.1 \div 0.15 \quad (4.57)$$

$$u_{max} = V_s(1 - \Delta D_{50}/z_{max}) \quad (4.58)$$

where  $D_{50}$  = characteristic grain diameter (m) and  $\Delta$  = relative density of the the bank protection material.

Note that the celerity of the front of the stern wave is equal to the ship speed. Equation 4.58 gives the maximum velocity of water particles in the stern wave.

As the ship speed increases, the stern wave may eventually break, depending on the local water depth (Figure 4.25). Then  $i_{max}$  is larger than 0.1 to 0.15 and the wave breaking causes an extra attack on the bank protection.

On top of this, propeller jets can create another attack on bed and bank protections. This is especially the case in bends and near unloading and holding quays. The jet is very turbulent and velocities can be very high (up to 10 m/s). When manoeuvring or starting from stationary, a vessel may therefore cause serious scour and protection failure.

The current velocity behind the stern wave, the so-called ‘wake’, is mainly caused by the return of water from the propeller jet. In extreme situations, with large sailing speeds and a small UKC ( $h_0/D_s < 1.2$ ) a very strong wake may occur. The maximum wake velocity in this situation might grow to a velocity even larger than the maximum return current velocity under the ship, as has been shown in experiments.



Figure 4.25: Stern wave breaking on a bank (images by Bundesanstalt fr Wasserbau (BAW) are licenced under CC BY-NC-SA 4.0).

#### 4.4.2 Transverse gradients in the water motion

So far, we have assumed the primary water motion to be uniform over the cross-section. This is only true if  $A_c/A_s$  is smaller than 5 (or  $W_s/B_s$  smaller than about 12). For larger values a gradient will occur and the water level depressions and return current velocities will decrease as the distance to the ship increases.

Based on potential flow theory one may estimate the transverse distribution of the current velocities and the water level depression, but at present this is done with numerical models (Figure 4.26).

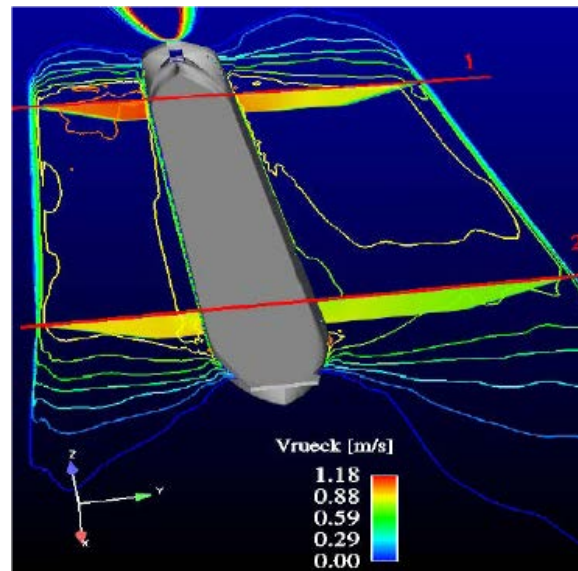


Figure 4.26: Computed gradient in return current next to the ship (image by Bundesanstalt für Wasserbau, Karlsruhe is licensed under CC BY-NC-ND 4.0).

#### 4.4.3 Flow velocities underneath the ship keel

Tunnels and pipelines crossing navigation canals or rivers cannot always be buried deep below the bed and may require a cover layer to protect the structure against the induced water motions below the ship keel (Figure 4.27). Also bed protections in harbours and approaches to locks are influenced by water motions caused by ships sailing over them (CIRIA; CUR; CETMEF, 2007).

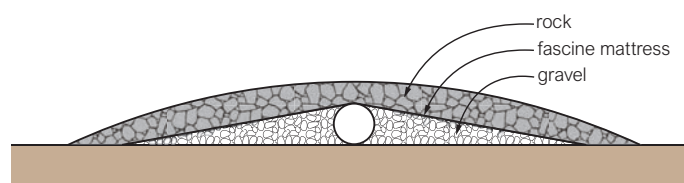


Figure 4.27: Protected pipeline crossing (by TU Delft – Ports and Waterways is licenced under CC BY-NC-SA 4.0).

The flow field underneath the ship's keel cannot be computed as if it were one-dimensional. The maximum flow velocity occurs below the bow where the height available to the flow is less than the under keel clearance. Figure 4.28 explains why.

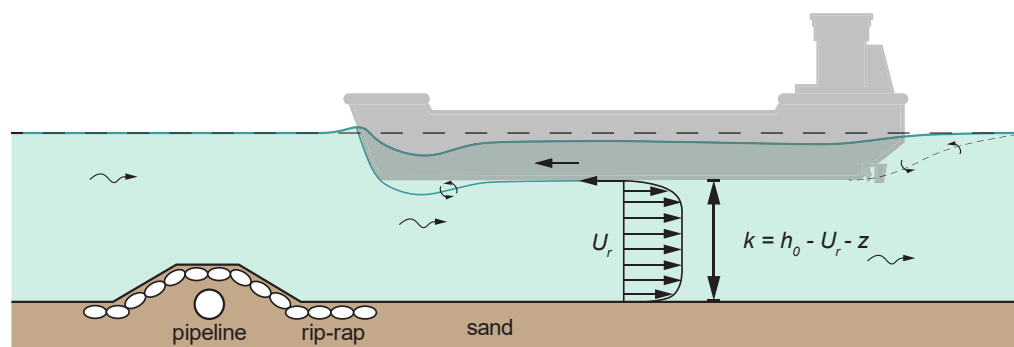


Figure 4.28: Schematic of the flow between ship and channel bed (by TU Delft – Ports and Waterways is licenced under CC BY-NC-SA 4.0).

Equation 4.59 gives a first estimate of the flow velocities underneath a ship (Dorst et al., 2016):

$$U_{rb} = cU_r \quad (4.59)$$

where  $c = 1.5$  to  $2.0$

Research at Delft Hydraulics (Stolker and Verheij, 2006) resulted in an improved version of the co called Maynard equation (also see Figure 4.29):

$$\frac{U_{rb}}{V_s} = 1.07 \left( \frac{B_s}{h_0} \right)^{0.08} \left( \frac{D_s}{h_0} \right)^{1.82} \quad (4.60)$$

in which  $U_{rb}$  is the return current velocity just outside the bed boundary layer. This velocity can be used to calculate the bed shear stress and the sediment transport rate. In case of a coarse sediment bed (sand or gravel) the transport gradients determine the local erosion. In case of finer sediment (fine sand, silt or mud) the shear stress directly determines the erosion rate:

$$\frac{dz_b}{dt} = \frac{M}{\rho_s g} \left( 1 - \frac{\tau_b}{\tau_{cr}} \right) \quad (4.61)$$

$$\tau_b = \frac{1}{2} c_f \rho_w U_{rb}^2 \quad (4.62)$$

in which:

- $z_b$  = bed level with respect to a fixed reference level [m],
- $t$  = time [s],
- $M$  = erosion coefficient [ $kg/(ms^3)$ ]
- $\tau_{cr}$  = critical shear stress for erosion [ $N/m^2$ ]
- $\tau_b$  = actual bed shear stress [ $N/m^2$ ]
- $c_f$  = friction coefficient [-]

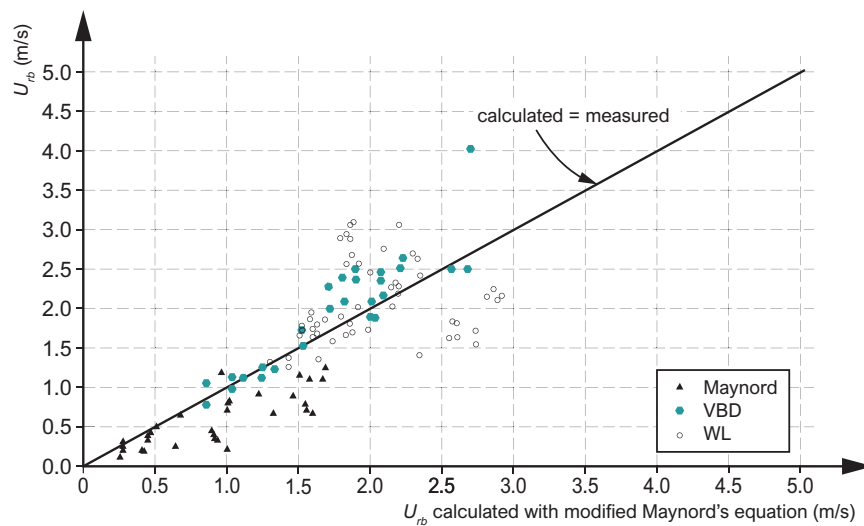


Figure 4.29: Computed and measured flow velocities under the keel (by TU Delft – Ports and Waterways is licenced under CC BY-NC-SA 4.0).

3-D numerical simulation models such as Delft3D can also be used to predict sediment transport and bed level effects of navigation. This concerns not only the effect of an individual vessel on the bed below it, but also the larger-scale effect of navigation on the sediment transport capacity of a river, for instance.

#### 4.4.4 Ship-induced water motions in rivers and groyne fields

So far we have assumed the channel banks to be straight and closed. Many regulated rivers, however, are bordered by groynes and groyne fields. The presence of groynes influences the flow, also outside the groyne fields. Figure 4.30 shows the flow pattern in a groyne field induced by a passing push-tow unit. It shows that if a large vessel or convoy passes a groyne at short distance this may result in strong eddies, in particular directly after passage of the stern (Figure 4.31).

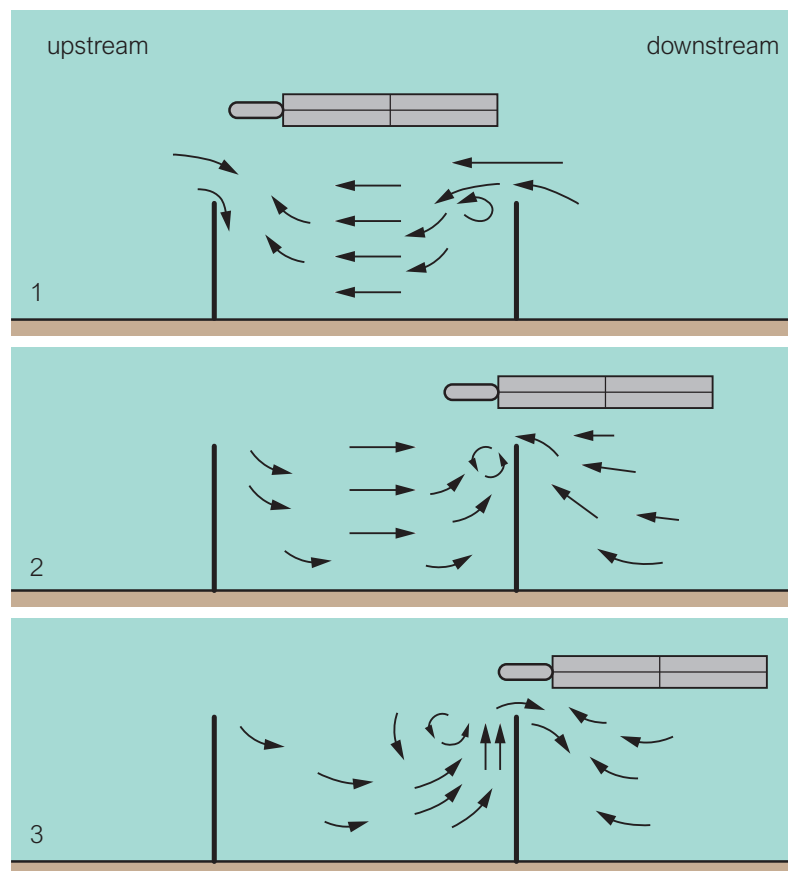


Figure 4.30: Flow in a groyne field induced by a passing four-barge unit (modified from Brolsma, 1988, by TU Delft – Ports and Waterways is licenced under CC BY-NC-SA 4.0).

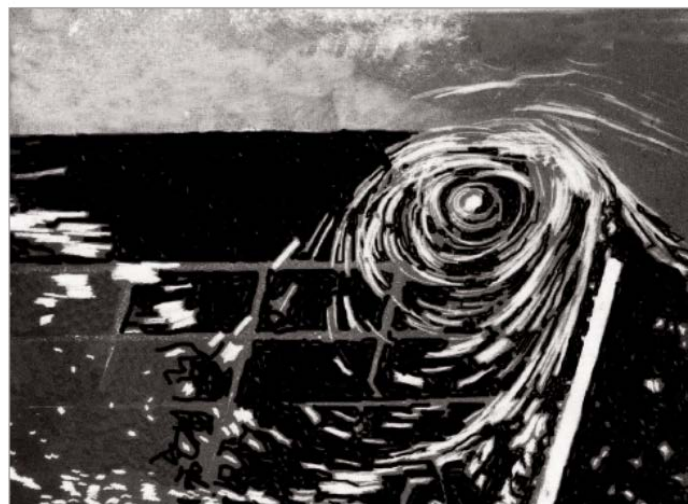


Figure 4.31: Eddy downstream of a groyne directly after passage (to the right) of a push-tow unit (Deltares (1987), verslag modelonderzoek Q93/Q576).

Clearly, the flow velocities around the head of a groyne can be very high. A first estimate of the velocities in a groyne field follows from the empirical equation (Termes et al., 1991; CIRIA; CUR; CETMEF, 2007):

$$\frac{|U_{local}|}{|U_c + U_r|} = \alpha \left( \frac{h_0}{h_{ref}} \right)^{-1.4} \quad (4.63)$$

in which:

- $U_{local}$  = maximum flow velocity at a location in the groyne field [m/s],
- $U_c$  = average flow velocity in the river [m/s],
- $U_r$  = average return velocity in front of the groyne head [m/s],
- $\alpha$  = coefficient depending on the location in the groyne field [-],
- $h_0$  = average water depth in the river [m], and
- $h_{ref}$  = average water depth in the river at the discharge at which the groynes submerge [m].

For the groyne fields along the Dutch Rhine branches, the value of  $\alpha$  varies between 0.2 and 0.6, but this does not necessarily apply to other rivers. The highest values are directly downstream of the head of a groyne.

#### 4.4.5 Hydrodynamic phenomena during overtaking

When a vessel is overtaking another, their return currents and the water-level depressions will reinforce each other. Therefore the water level will decrease more between the two ships than between ship and bank. The ships will experience more resistance, and as the overtaking manoeuvre proceeds, they will be drifting towards each other due to the difference in hydrostatic pressure (Figure 4.32).

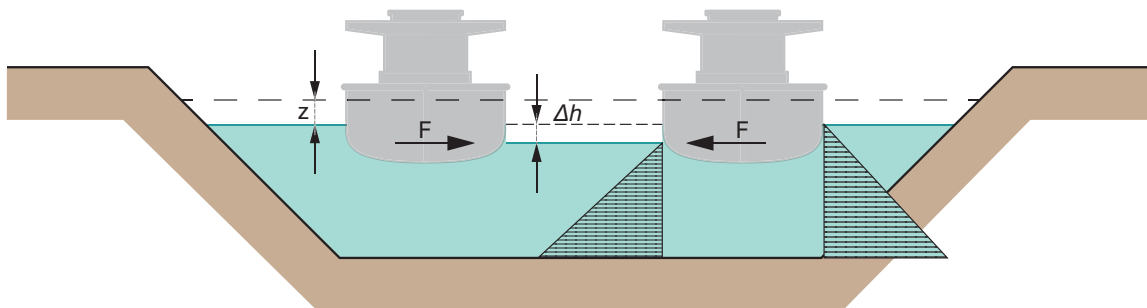


Figure 4.32: Hydrostatic pressure during overtaking (by TU Delft – Ports and Waterways is licenced under CC BY-NC-SA 4.0).

In an overtaking manoeuvre the navigator must pay close attention in order to stay in control, although the risks involved depend on the space available, of course.

The overtaking manoeuvre can be successfully completed if the ship to be overtaken strongly reduces her speed and the overtaking ship sails at an adjusted speed, so as not to be sucked against the other ship. However, reducing the speed of the ship to be overtaken must not lead to insufficient rudder pressure for manoeuvrability. In practice, overtaking is only feasible if the difference in speed between the two ships is more than 5 km/h.

The overtaking ship has to overcome two hydrodynamic barriers during the manoeuvre. The first barrier to overcome is at the start of the manoeuvre (Figure 4.33). The overtaking ship suddenly encounters a much smaller wet cross-section, with area  $(A_c - A_{s,1} - W_s z_1)$  due to the space occupied by the ship to be overtaken ( $A_{s,1}$ ) and the water level depression ( $z_1$ ) it causes. Moreover, the overtaking ship has to negotiate the extra return current ( $U_{r,1}$ ) caused by the ship to be overtaken.

The smaller flow section and the extra return current reduce the limit speed of the overtaking ship ( $V_{lim,2}$ ), whereas it has to remain higher than the actual speed of the ship to be overtaken. In reality, this is usually not a problem, because, due to the extra water level depression and return current, the speed of the ship to be overtaken will strongly decrease once the overtaking ship is next to her.

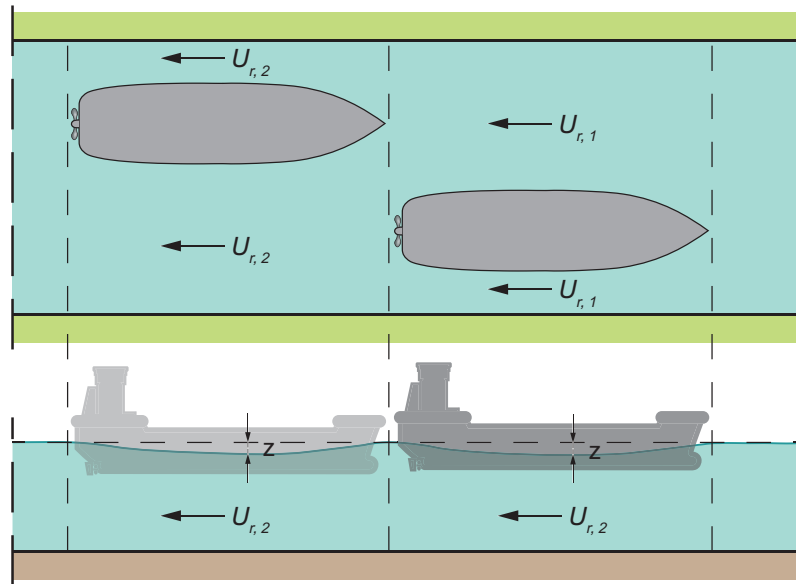


Figure 4.33: First barrier when overtaking (by TU Delft – Ports and Waterways is licenced under CC BY-NC-SA 4.0).

The second barrier occurs when the bow of the overtaking ship has just passed the other ship's bow (Figure 4.34). The bow of the former is then in an area of water level depression caused by itself, while the stern is still in the area of combined water level depression. The ship has to overcome the extra trim this causes, which requires extra power. If the overtaking ship does not dispose of this, she will lose speed and the overtaking manoeuvre will slow down or even fail.

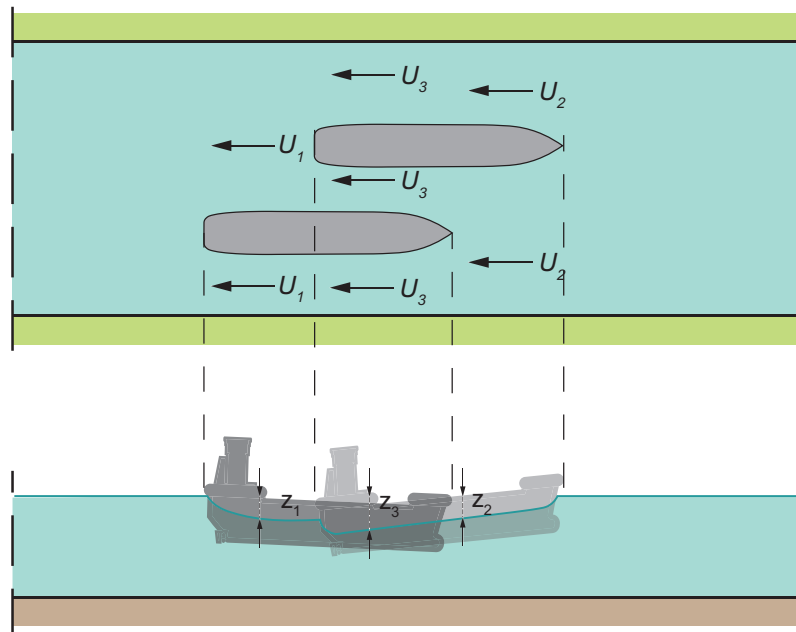


Figure 4.34: Second barrier when overtaking (by TU Delft – Ports and Waterways is licenced under CC BY-NC-SA 4.0).

The opposite applies to the ship that is overtaken: the bow is in an area of combined water level depression and the stern has only the ship's own water level depression. This generates a positive trim and a forward directed force, which will cause an increase of the ship's speed.



It may happen that the two ships come to sail as one system with the same speed, the so-called group speed. In that case the overtaking ship drags the slower ship along in their common water level depression. This may cause the overtaking manoeuvre to fail. For the overtaking manoeuvre to be successful, the slower ship must to reduce its speed.

The channel cross-section should be dimensioned for situations in which such a speed reduction is necessary. This may require a significantly larger profile than in the situation where no overtaking is allowed. Note that, nevertheless, the overtaking ship must still have sufficient power to overcome the second barrier.

In principle, it is possible to compute the individual ship speeds, the duration of the overtaking manoeuvre and the hydrodynamic phenomena (return current and water level depression) with the Schijf method. Janssen and Schijf (1953) give results of a number of laboratory tests on overtaking. Nowadays, it is more convenient to use Computational Fluid Dynamics (CFD) models for this purpose, of which Section 4.6 gives an example.

#### 4.4.6 Water motions in locks due to emptying or filling of the lock chamber

Emptying or filling of a lock chamber can be realized in three ways:

1. by opening sluices in the gates (possible in all three variants);
2. by opening the valves in bypass or longitudinal drains that discharge water through one or more openings in the chamber walls or the chamber floor;
3. by slightly lifting or tilting the gate (a vertical lift or pivot gate, for instance) and allowing water to pass by.

When filling the chamber the energy dissipation inside the chamber is considerable, as the flow decelerates rapidly. This can cause great inconvenience to the vessels in the chamber, especially if it is fi

lled fast. When emptying the chamber, i.e. the outgoing flow accelerates and suppresses turbulence, which is less of an inconvenience to the vessels. When decelerating outside the chamber, the flow is highly turbulent, again, and may cause erosion. To prevent this, bed protection structures are applied.

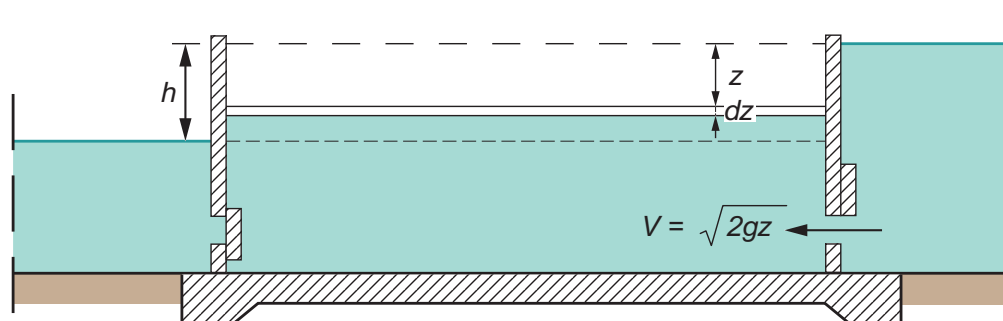


Figure 4.35: Chamber filling by means of sluices in the gates (by TU Delft – Ports and Waterways is licenced under CC BY-NC-SA 4.0).

#### Filling and emptying time in case of slowly varying water levels

If the sluice (opening area  $A_{sl}$  [m<sup>2</sup>]) is suddenly opened, the water discharge entering the chamber, the time-dependent filling discharge  $Q_f(t)$ , will be

$$Q_f(t) = mA_{sl}\sqrt{2gz(t)} \quad (4.64)$$

in which the discharge coefficient  $m$  depends on the shape and curvature of the discharge opening and will vary between 0.6 and 0.9. If the surface area of the chamber is  $A_{ch}$  [m<sup>2</sup>], mass conservation requires:

$$A_{ch}dz = -mA_{sl}dt\sqrt{2gz} \quad (4.65)$$

(note that  $z$  decreases as the chamber fills up). Integrating this over time, with initial condition

$$z(t = 0) = H \quad (4.66)$$

yields (Figure 4.36):

$$z(t) = \left[ \sqrt{H} - \frac{m A_{sl} \sqrt{2g}}{2A_{ch}} t \right]^2 \quad (4.67)$$

Then the total filling time  $T$  (when  $z = 0$ ) follows from:

$$T = \frac{2A_{ch} \sqrt{H}}{m A_{sl} \sqrt{2g}} \quad (4.68)$$

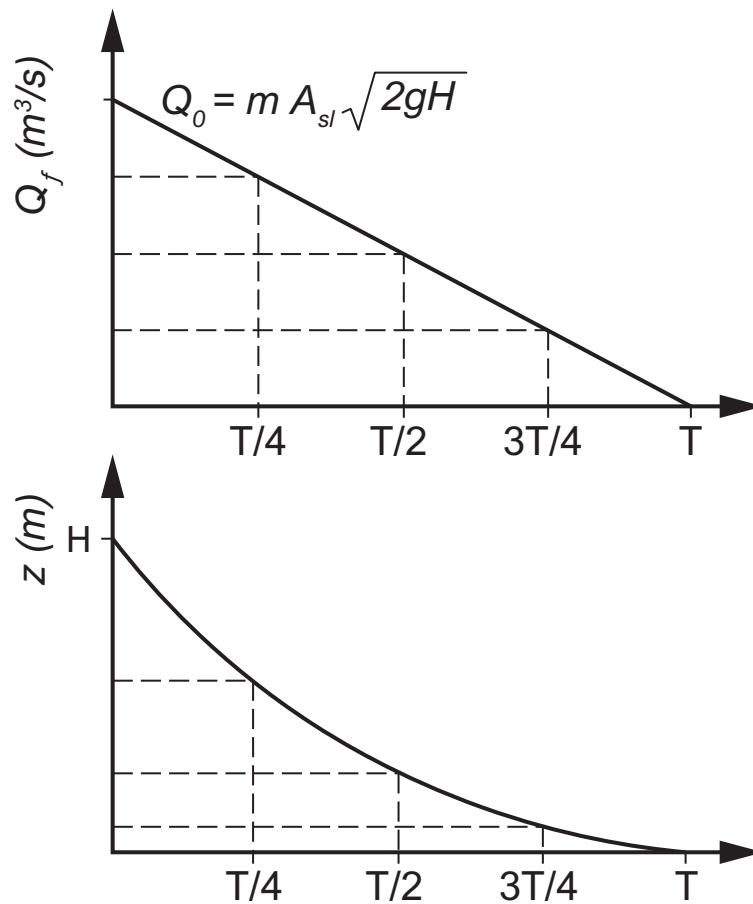


Figure 4.36: Slow chamber filling process if the sluice is opened suddenly (by TU Delft – Ports and Waterways is licenced under CC BY-NC-SA 4.0).

### Filling and emptying time in case of translatory waves

In the previous paragraphs we assumed the level in the lock chamber to rise gradually over the entire chamber area. In reality, however, a translatory wave will run up and down the chamber if the sluice is suddenly opened. As a consequence, the lock chamber will be filled in ‘slices’ (Figure 4.37).

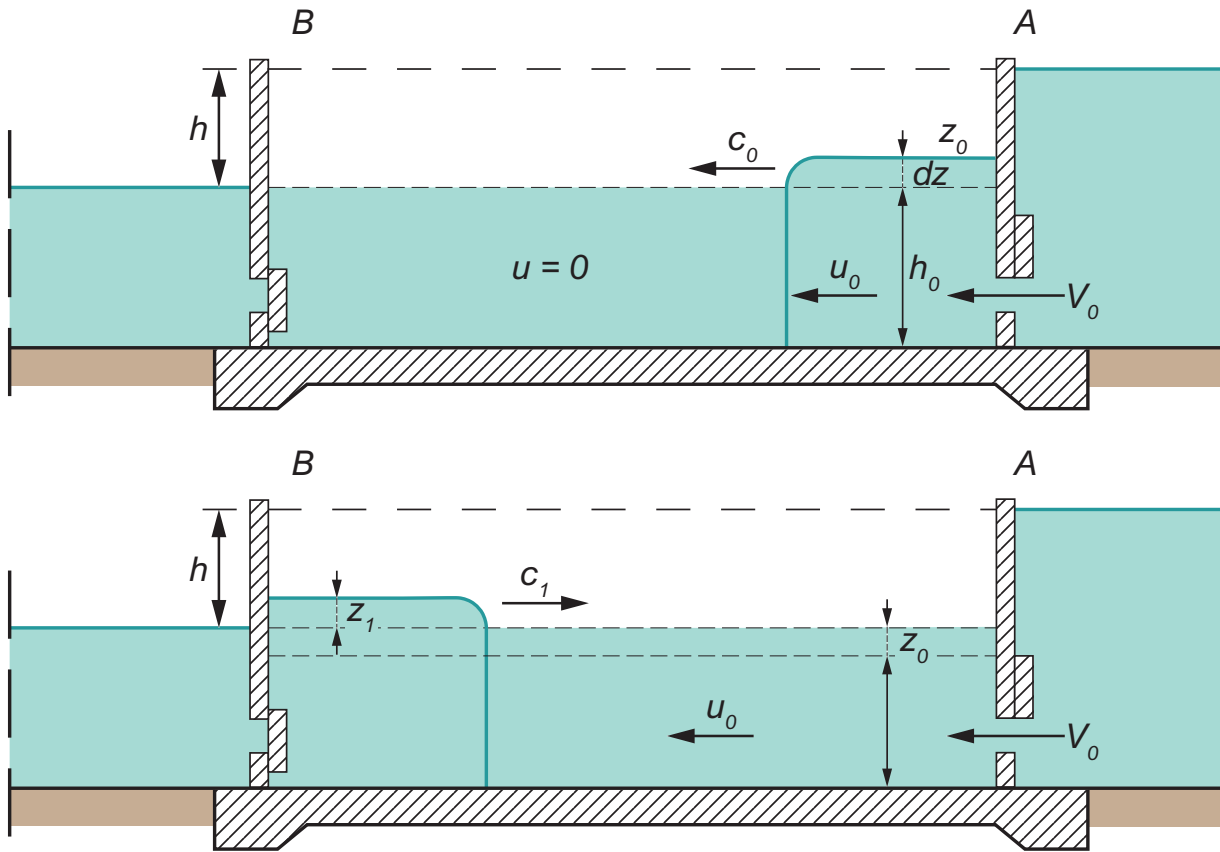


Figure 4.37: Translation wave during lock filling (by TU Delft – Ports and Waterways is licenced under CC BY-NC-SA 4.0).

At time  $t = 0$  a positive translatory wave of height  $z_0$  begins to propagate from A to B (Figure 4.37). Initially, there will be an equally high negative wave propagating from the other side of the gate away from the lock. The lock approach area is assumed to be so much wider than the lock entrance, that this effect can be ignored after some time. Then the propagation speed of the first translatory wave in the chamber is

$$C_0 = \sqrt{g(h_0 + z_0)} \tag{4.69}$$

The discharge through the sluice determines the height of the wave. Mass conservation requires:

$$Q_f = C_0 z_0 W_l = mA_{sl} \sqrt{2g(H - z_0)} \tag{4.70}$$

When this wave reaches the end of the lock, it bounces against gate B. The returning wave of height  $z_1$  has a propagation speed

$$C_1 = \sqrt{2g(h_0 + z_0 + z_1)} \tag{4.71}$$

where the wave height follows from mass conservation, again:

$$Q_f = C_1 z_1 W_l = mA_{sl} \sqrt{2g(H - z_0)} \tag{4.72}$$

et cetera.

Figure 4.38 shows schematically the filling process due to a translatory wave. Note that the sluice discharge only changes every time the bounced wave reaches gate A again. Also note that the wave height decreases as the lock chamber fills up.

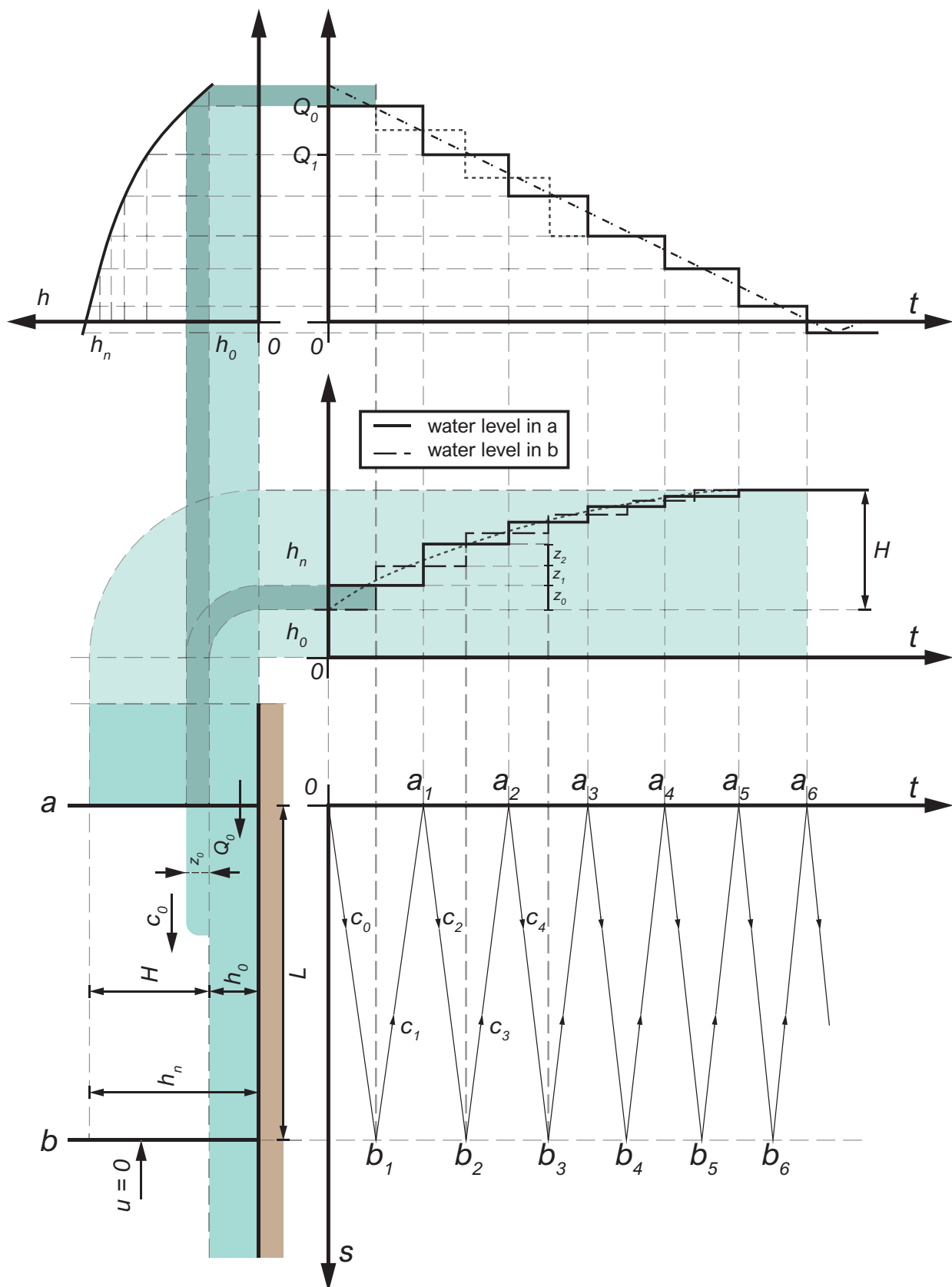


Figure 4.38: Lock chamber filling with translation waves (by TU Delft – Ports and Waterways is licenced under CC BY-NC-SA 4.0).

If there are ships in the lock chamber, a completely different situation occurs. A complex system of hydraulic forces on the ships creates large hawser forces, extra reflections of the translation wave against the ships and a more complex velocity field (Figure 4.39).

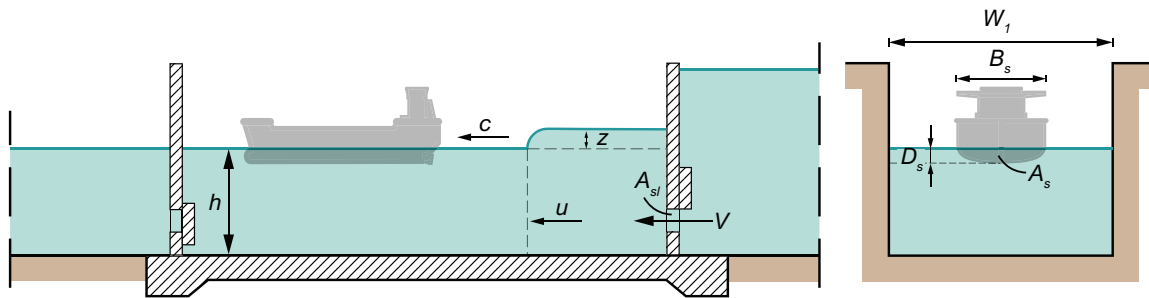


Figure 4.39: Translation wave in a lock chamber with a ship (by TU Delft – Ports and Waterways is licenced under CC BY-NC-SA 4.0).

Even though the situation is more complex, the translation waves are recognisable in the time-variation of the hawser forces: they keep on changing sign, more or less at the frequency of the wave front passages (Figure 4.40). Further see Part IV – Section 4.3 for how these hawser forces can be dealt with.

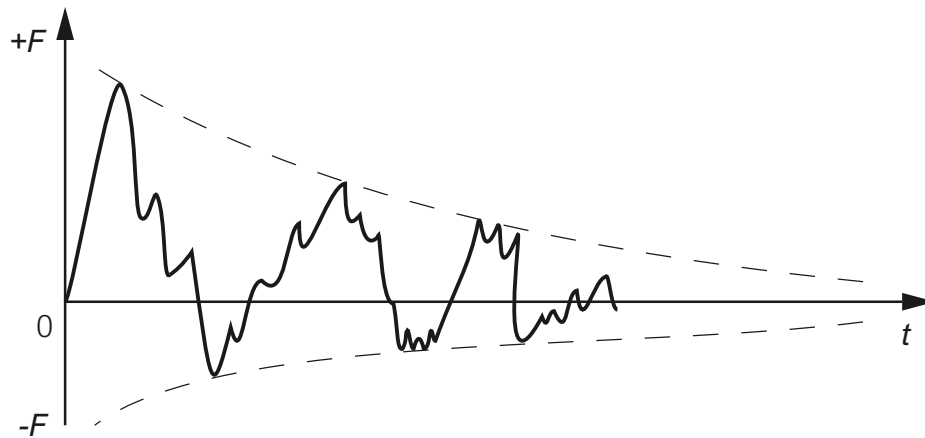


Figure 4.40: Observed time-evolution of a hawser force (by TU Delft – Ports and Waterways is licenced under CC BY-NC-SA 4.0).

**Filling or emptying the chamber by gradually opening the sluice**

Hawser forces can be reduced by opening the sluice more gradually. If the sluice is opened at a constant speed, a rectangular opening will increase linearly with time (Figure 4.41).

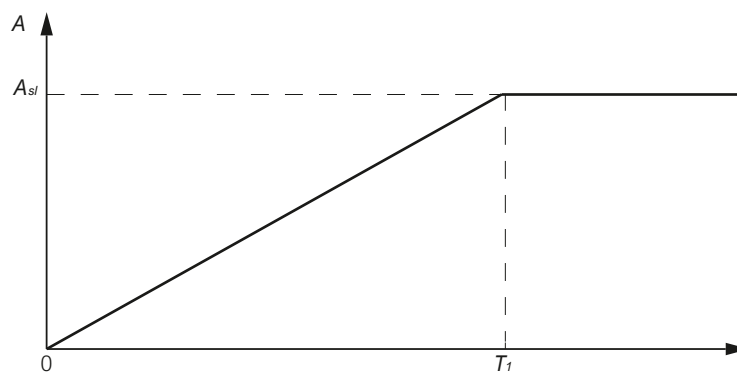


Figure 4.41: Linear sluice opening process (by TU Delft – Ports and Waterways is licenced under CC BY-NC-SA 4.0).

If the sluice is opened linearly over time  $T_1$  and the chamber fills evenly without translation waves, continuity requires (see [Figure 4.37](#) for symbol definitions):

$$A_{ch}dz = -mA_{sl}\frac{t}{T_1}\sqrt{2gz}dt \quad (4.73)$$

whence, with initial condition ([Equation 4.67](#)):

$$z(t) = \left( \sqrt{H} - \frac{mA_{sl}\sqrt{2g}}{4A_{ch}T_1}t^2 \right)^2 \quad (4.74)$$

for  $0 < t < T_1$ . At the end of the sluice opening procedure we have

$$z(T_1) = \left( \sqrt{H} - \frac{mA_{sl}\sqrt{2g}}{4A_{ch}}T_1 \right)^2 \quad (4.75)$$

The remaining level difference  $H - z(T_1)$  is filled up in the same way as in the case of sudden opening,

$$z(t) = \left( \sqrt{zT_1} - \frac{mA_{sl}\sqrt{2g}}{2A_{ch}}(t - T_1) \right)^2 = \left( \sqrt{H} - \frac{mA_{sl}\sqrt{2g}}{2A_{ch}}\left(t - \frac{1}{2}T_1\right) \right)^2 \quad (4.76)$$

Then total filling time becomes:

$$T = \frac{T_1}{2} + \frac{2A_{ch}\sqrt{H}}{mA_{sl}\sqrt{2g}} \quad (4.77)$$

So the total filling time increases with half the sluice opening time, as compared to the case of a sudden sluice opening.

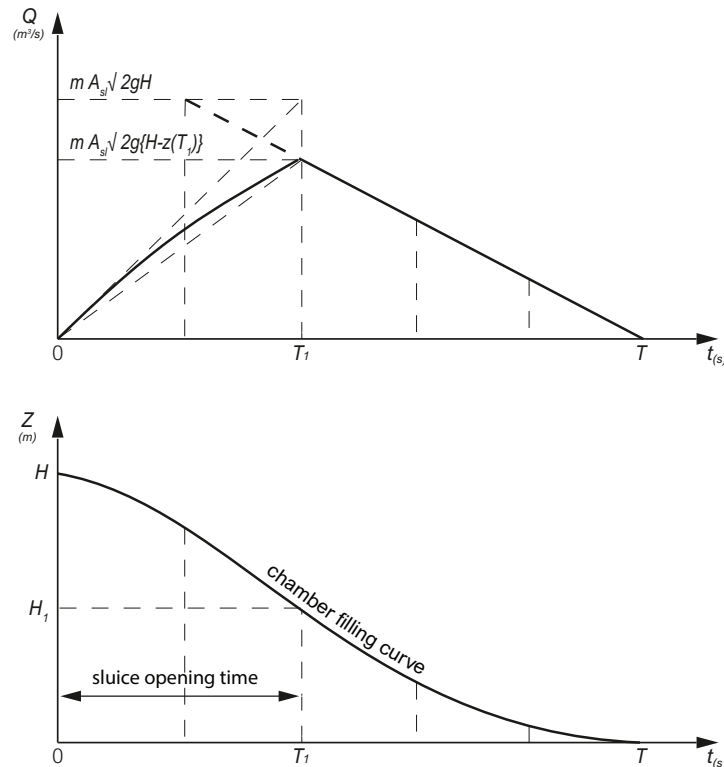


Figure 4.42: Lock chamber filling with a gradually opened sluice (by TU Delft – Ports and Waterways is licenced under CC BY-NC-SA 4.0).

Figure 4.42 shows the time evolution of the filling process. Figure 4.36, Figure 4.38 and Figure 4.42 all show that the filling rate considerably slows down towards the end of the process. That is why in practice the gates are opened before the entire head difference has been levelled out. This can save a significant amount of time.

#### 4.4.7 Ship-induced translation waves

In the transition between the lock approach and the relatively narrow lock a ship encounters changes in return current, water-level depression and resistance. A sudden transition in cross-sectional area gives rise to the following phenomena:

- the return current velocity along the ship increases significantly, as does the waterlevel depression,
- a positive translation wave enters the lock chamber;
- a negative translation wave propagates into the lock approach area.

The greater the ship's speed and the greater the transition in blockage factor, the stronger these phenomena become (see Figure 4.43 and Figure 4.44).

During the actual lock entry, the navigation speed and the associated hydrodynamic phenomena may become quite irregular (Figure 4.43). In practice, however, this gives little cause for concern as long as the blockage factor is  $A_s/W_l h < 0.4$ .

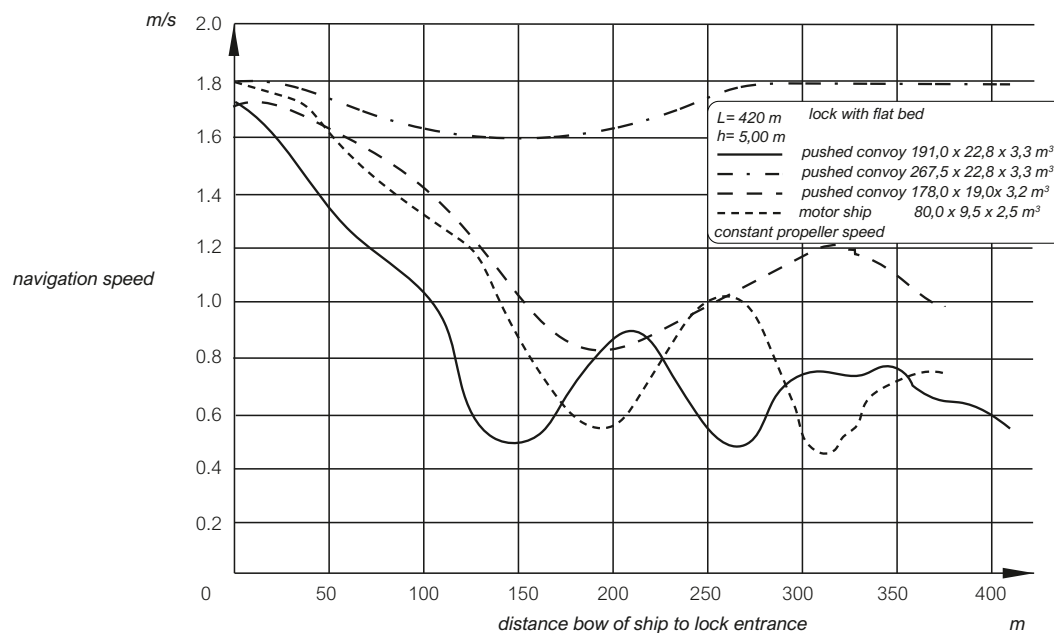


Figure 4.43: Navigation speed when approaching and entering a lock (Kooiman, 1973). Image by TU Delft – Ports and Waterways is licenced under CC BY-NC-SA 4.0.

Another problem arises with loaded push convoys in push convoy locks and the largest maritime vessels in maritime locks, which can have blockage factors up to 0.8. Their initial speed ( $V_0$ ) may not be too large, otherwise the translation waves created by them may cause damage to the closed gates the first time they rebound. The maximum height of the translation wave ( $Z_{max}$ ) appears to be directly proportional to the square of the initial vessel speed and the ratio of the midship cross-sectional area ( $A_s$ ) and the remaining cross-sectional area ( $W_l h_0 - A_s$ ) through which the return current takes place. According to Figure 4.44, the coefficient of proportionality is approximately 1.44, so:

$$\frac{Z_{max}}{h_0} = 1.44 \frac{V_0^2}{gh_0} \frac{A_s/A_{lock}}{1 - A_s/A_{lock}} \quad (4.78)$$

in which  $A_{lock} = W_l h_0$  and  $h_0$  is the water depth in the lock chamber or above the entrance threshold, depending on the case considered.

In principle, Equation 4.78 shows some resemblance with the value  $z_{max}$  that can be computed with the Schijf method, with Equation 4.6 for a ship sailing in a canal, but instead of  $A_s/A_c$  now the value of  $A_s/A_{lock}$  is applied.

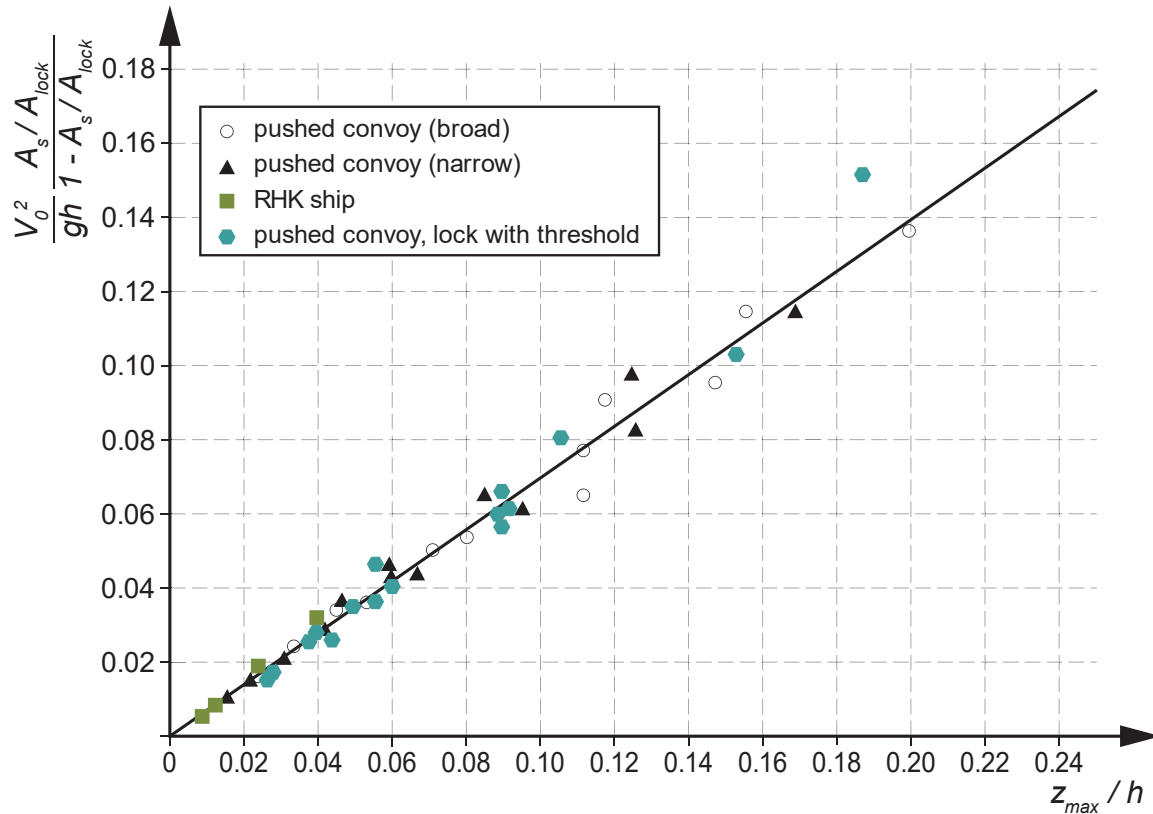


Figure 4.44: Maximum ship-induced translation wave height at the closed lock head (Kooman, 1973). Image by TU Delft – Ports and Waterways is licenced under CC BY-NC-SA 4.0.

## 4.5 Ship speed and ship resistance

The speed of a ship mainly depends on the resistance encountered while sailing, and of course on the installed engine power transferred by the propeller. The speed chosen is a trade-off between travelling time, transport costs and on time cargo delivery. Much research has been done on this subject, because it enables ship owners to obtain important management information, such as energy consumption and travel time per trip, and the number of ships needed for a certain throughput. Relevant research, including field tests, has been done in Germany. In the Netherlands MARIN played a significant role, though primarily focusing on optimising the shape of the ship's hull. Delft Hydraulics came up with equations to predict the ship's speed (Van de Kaa, 1978). A comprehensive overview is presented by Pompée (2015).

In principle, the ship speed on restricted water follows from:

$$P_b \eta_T = R_T (V_s + U_r) \quad (4.79)$$

in which:

- $P_b$  = effective power [kW],
- $\eta_T$  = total efficiency factor [-],
- $R_T$  = total resistance [kN],
- $V_s$  = ship speed [m/s],
- $U_r$  = return current [m/s].



The applied power is not the full installed power, because about 10% is used for systems on board such as lighting, heating, et cetera. Furthermore, there are various losses in the system (see Figure 4.45). The total energy loss is the sum of all individual components. The efficiency factor  $\eta_T$  typically has a value of 0.7.

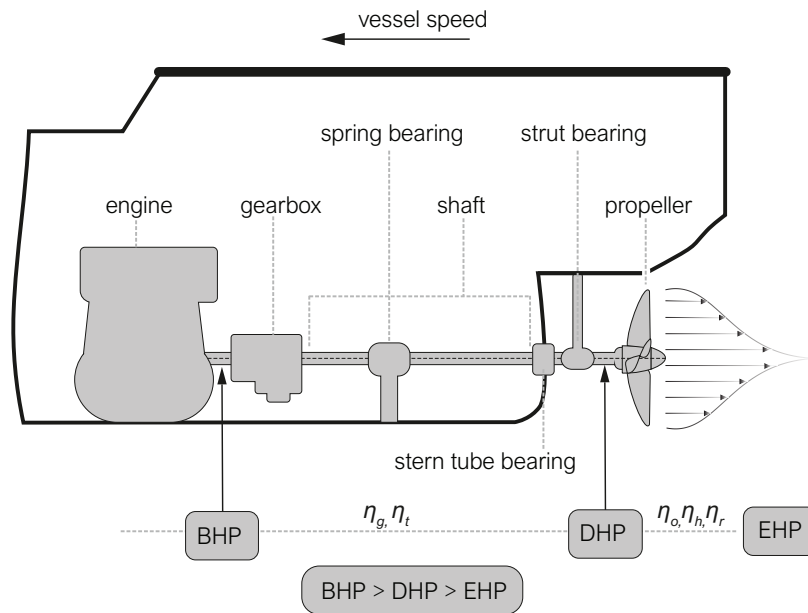


Figure 4.45: Schematic of the different power components and efficiency factors (by TU Delft – Ports and Waterways is licenced under CC BY-NC-SA 4.0).

The total resistance  $R_T$  encountered by a sailing ship is strongly determined by the geometry of ship and waterway and the previously described interaction between the two. Especially in restricted water, most of the resistance is caused by the water movement around the ship. Sinkage and trim play a role here, but in a first approximation of the relationship between deployed engine power and ship speed we assume the sinkage to be equal to the water level depression and trim to be absent.

The resistance, expressed as a force, consists basically of two components: frictional resistance and pressure or wave resistance (Figure 4.46). There are more components, such as the resistance caused by a bulb at the bow and the resistance due to appendages such as rudders and propellers, but they are generally of secondary importance. For a detailed overview, see Part IV – Section 5.1.

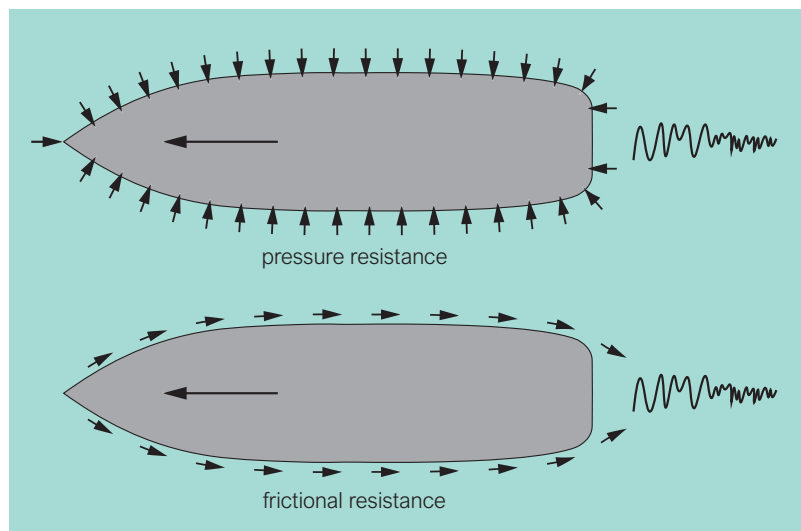


Figure 4.46: Frictional and pressure resistance (by TU Delft – Ports and Waterways is licenced under CC BY-NC-SA 4.0).

- (a) *Frictional resistance* is caused by friction forces, acting tangentially on the surface of the submerged part of hull. If a ship sails in unconfined water without an ambient current, this part of the resistance is proportional to the ship's speed squared and its wetted surface area,  $S$ :

$$R_f = \frac{1}{2}\rho_w V_s^2 C_f S \quad (4.80)$$

In restricted water the return current and the water-level depression cause a significant part of the resistance of moving ships. This is taken into account via

$$R_f = \frac{1}{2}\rho_w (V_s + U_r)^2 C_f S \quad (4.81)$$

So here the ship's speed relative to the surrounding water is the determining factor. The friction coefficient  $C_f$  depends on parameters such as the roughness of the hull and the shape and dimensions of the ship. If no further information is available, a value of 0.002 is often a good first estimate. For old ships with a lot of fouling higher values may apply.

- (b) *Pressure resistance* – is caused by differences in water pressure on the submerged part of the hull. Water pressure is omnidirectional, but the difference between bow and stern may give rise to a net longitudinal component causing resistance against the ship's forward motion. This pressure resistance is approximately proportional to the wet amidships cross-section and the ship's speed squared:

$$R_p = \frac{1}{2}\rho_w V_s^2 C_p A_s \quad (4.82)$$

The pressure resistance increases as the waterway becomes more restricted, due to the increased sinkage and trim of the ship associated with the larger water level depression. The drag coefficient  $C_p$  depends on the shape and the (underwater) dimensions of the ship. A typical value is 0.1, but values up to 0.3 have been found for loaded pusher tugs, depending on the number of push-barge units.

[Van de Kaa \(1978\)](#) has introduced a simplified equation to determine the total resistance  $R_T$  of push-barge units in restricted water:

$$R_T = \frac{1}{2}\rho_w (V_s + U_r)^2 C_f S + \frac{1}{2}\rho_w V_s^2 C_p A_s + \rho_w g A_s z \quad (4.83)$$

The extra term accounts for the fact that in case of a push-barge unit the propeller is at a small distance behind the barges. In case of a conventional ship the propeller is at the stern, where water-level depression is no longer present. The basic assumption is that the thrust produced by the propeller is used entirely to overcome the pressure and frictional resistances, so as not to generate the secondary hydrodynamic phenomena around the moving ship.

Resistance may also be increased if a vessel sails closely to a bank, for instance when it encounters another ship, or is overtaken by one. The return current between the vessel and the bank will increase and thereby the water-level depression and the sinkage. This slows down the vessel, commonly by some 5 to 10%. If in case of an emergency the ship has to navigate very close to the bank, the speed reduction may increase to 15 to 20%.

For conventional vessels and tugs, the total resistance can be estimated with the following set of empirical equations derived by Gebers (in [Graewe, 1967](#)):

$$R_T = \rho_w g (C_p A_s + C_f S) (V_s + U_r)^{2.25} \quad (4.84)$$

$$S = \nabla^{1/3} (3.4 \nabla^{1/3} + 0.5 L_s) \quad (4.85)$$

$$\nabla = C_B L_s B_s D_s \quad (4.86)$$

The block coefficient depends on the ship type. Typical values are 0.9 for conventional ships and 0.75 for tugs.

The coefficients  $C_p$  en  $C_f$  depend on the draught:

$$\begin{aligned} C_p &= 3.5 \cdot 10^{-3} \text{ for a loaded ship,} \\ C_p &= 2.0 \cdot 10^{-3} \text{ for an unloaded ship,} \\ C_f &= 0.14 \cdot 10^{-3} \text{ for loaded and unloaded ships.} \end{aligned}$$

Because the return current velocity and the water-level depression are functions of  $V_s$ , this speed cannot be derived straightforwardly. Given the propulsion power and the efficiency factor, it has to be determined through an iterative procedure using Schijf's method, for instance. Test results (Van de Kaa, 1978) showed that for a given value of the energy power the computed speeds of push-tow units deviated less than 10% from the measured ones. Only for channel widths that were small relative to the ship length deviations increased rapidly.

### Ship speed

Computations with the equations above finally result in maximum ship speed attainable with the installed engine power. The computed speed should be less than the limit speed, as presented earlier in this chapter and summarised below.

According to the Schijf method, the limit speed in a width- and depth-limited channel follows from (see Equation 4.9):

$$\frac{V_{lim}}{\sqrt{gh}} = \left[ \frac{2}{3} \left( 1 - \frac{A_s}{A_c} + \frac{1}{2} \frac{V_{lim}^2}{gh} \right) \right]^{\frac{3}{2}} \quad (4.87)$$

In a waterway that is only depth-limited the limit speed follows from (combine Equation 4.29 and Equation 4.31):

$$V_{lim} = \sqrt{\frac{gL_s}{2\pi} \tanh\left(\frac{2\pi h_0}{L_s}\right)} \quad (4.88)$$

At open sea or very wide and deep waterways the limit speed reads (see Equation 4.29)

$$V_{lim} = \sqrt{\frac{g}{2\pi} L_s} \quad (4.89)$$

The limit speed according to Equation 4.89 is often called the hull speed. With  $g = 9.81 \text{ m/s}^2$  this becomes:

$$V_{lim} = 1.25\sqrt{L_s} \text{ in m/s, or } V_{lim} = 4.5\sqrt{L_s} \text{ in km/hr, or } V_{lim} = 2.43\sqrt{L_s} \text{ in knots.}$$

These limit speeds are applicable to water-displacement ships only. This type of ships cannot pass the Froude limit 1. Fast ferries or fast yachts can, because they can plane. The Ocean Race yachts, for instance, have a length of 19.85 m, which means that their top speed (speed over water) according to Equation 4.89 is about 20 km/hr. Yet, during the race in 2019 one of the yachts sailed 600 miles in in 24 hours, which is an average speed 45 km/hr (speed over ground). This difference is not likely to be explained by a strong following ocean current.

Equation 4.89 can also be rewritten in terms of a Froude number based on the ship length, a quantity often used in marine engineering:

$$Fr_L = \frac{V_s}{\sqrt{gL_s}} \quad (4.90)$$

This yields a limit Froude number of  $1/\sqrt{2\pi} = 0.4$ .

Figure 4.47 shows the relation between the limit Froude number and the ratio  $h_0/L_s$  for various values of the blockage factor. The deep-water limit value of 0.4 can clearly be seen for small values of  $A_s/A_c$ .

Generally, ships sail at about 70 to 85% of the limit speed, as above these values the wave or pressure resistance increases rapidly.

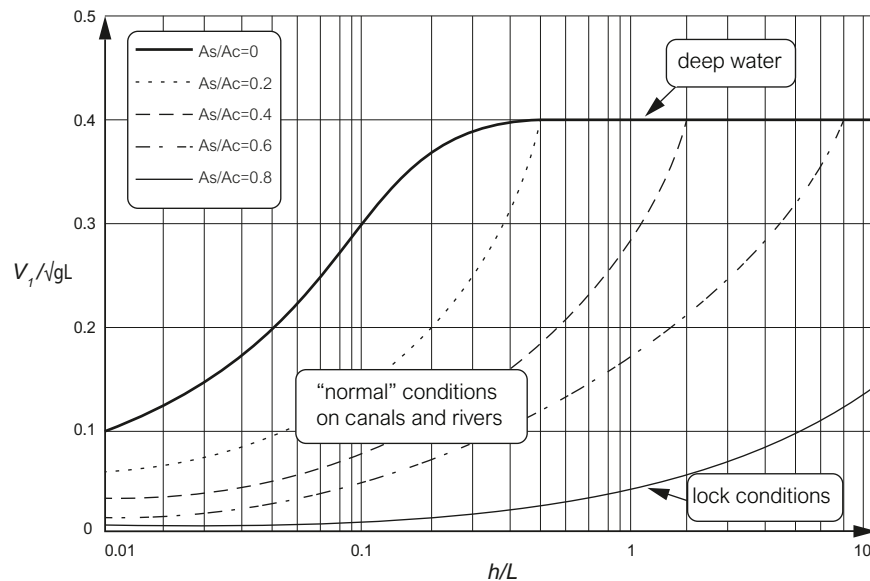


Figure 4.47: Relation between the limit Froude number and  $h_0/L_s$  (by TU Delft – Ports and Waterways is licenced under CC BY-NC-SA 4.0).

## 4.6 Numerical simulations

In the preceding sections we have presented analytical methods to describe the ship-induced water motion. Of course, it is also possible to compute the ship-induced primary water motion with CFD models, using software systems such as Delft3D (Deltares), Mike software (DHI), FINEL2D (Svasek Hydraulics), or HVEL2D (USACE-WES). These models are based on shallow water approximations (hydrostatic pressure distribution) and therefore describe the primary water motion. They are not suitable, however, to describe the secondary water motion. Figure 4.48 presents an example of a result of computations with FINEL2D. The ship is simulated by imposing a pressure distribution at the location of the ship, such that the water-level assumes the form of the underwater part of the ship. The picture shows the water-level depression and the flow field around the ship.

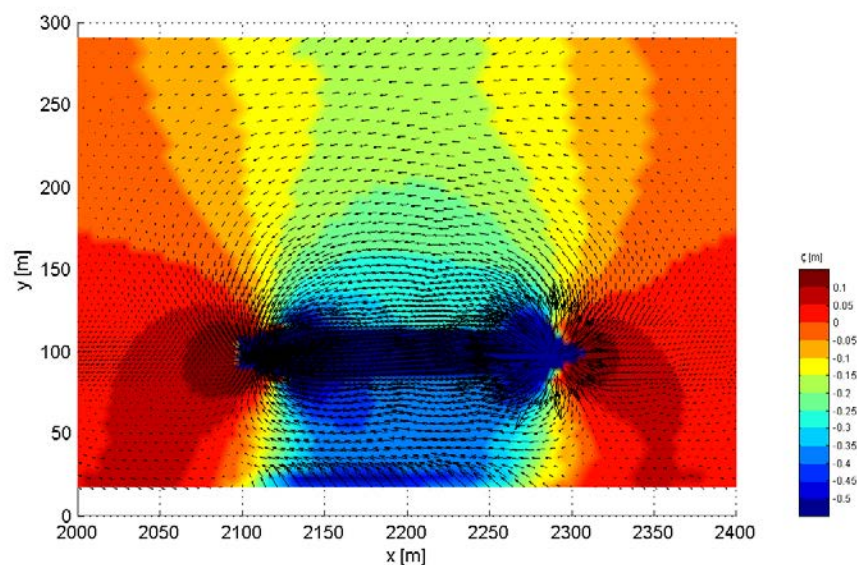


Figure 4.48: Water-level depression and velocity field around an eccentrically sailing ship (from red to blue: increasing water level depression). Image by TU Delft – Ports and Waterways is licenced under CC BY-NC-SA 4.0.

Figure 4.49 shows an example obtained with Delft3D of the flow velocities during an overtaking manoeuvre. Note the strong return currents, with velocities up to 2.5 m/s when the stern of the overtaking vessel is approaching the bow of the overtaken vessel.

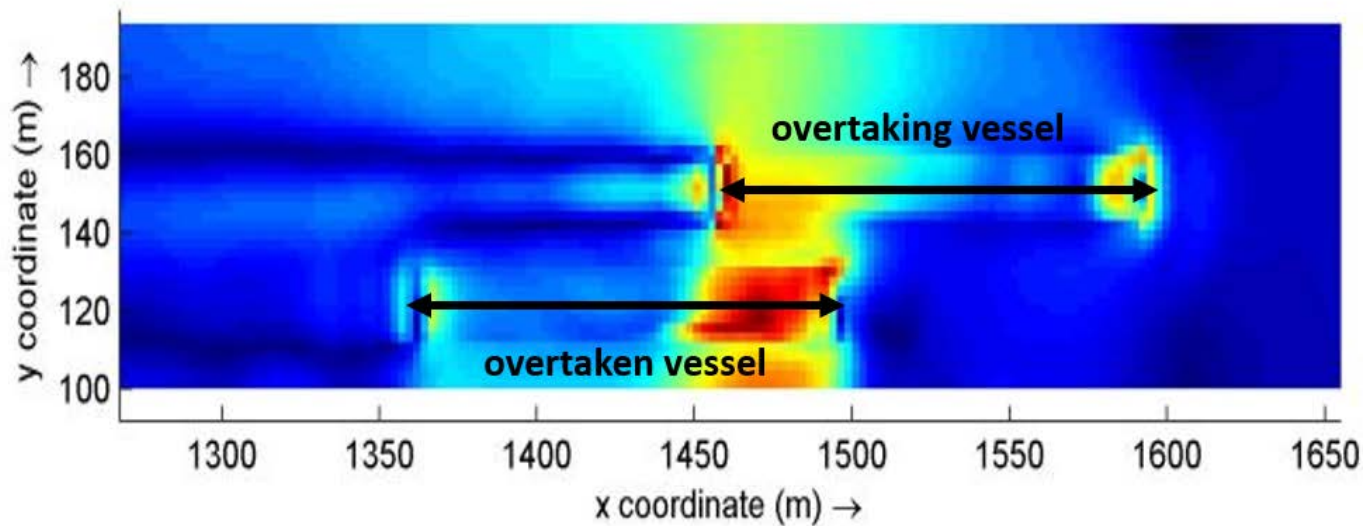


Figure 4.49: Simulation with Delft3D of two ships in an overtaking manoeuvre (image by Deltares is licenced under GNU General Public License).

Numerical simulation of the combined primary and secondary ship-induced water motion essentially includes simulation of wave generation and propagation, i.e. non-hydrostatic pressure. The Maritime Research Institute Netherlands (MARIN) has developed RAPID, a software system for the modelling of ship-induced wave generation, and Deltares has developed TRITON for wave propagation. Together these institutions initiated a study to investigate whether a combination of the two could do the job.

RAPID computes waves and currents induced by a sailing ship, thereby enabling variation in the modelling of aspects such as sailing speed, ship's dimensions and dimensions of the waterway. However, since RAPID was developed primarily to support ship design, it focuses on the near field, i.e. the area relatively close to the ship's hull. Consequently, RAPID does not include aspects such as refraction, diffraction and dissipation. Therefore, the results of RAPID have been used as input to TRITON. TRITON is based on the Boussinesq wave equations and has been developed to model propagation of shallow water waves, including features such as diffraction, refraction, wave-wave interaction and shoaling. Figure 4.50 shows the first result of the combined approach. They clearly show the primary and secondary water motion.

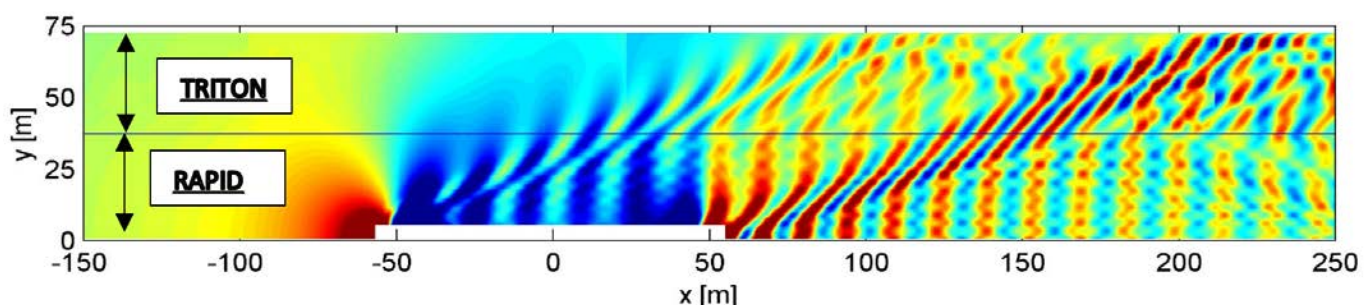


Figure 4.50: Ship-induced velocity pattern resulting from the combination of RAPID and TRITON (blue colours represent water level depressions and red colours water level elevations) (Verheij et al., 2001).

The effects of a sudden channel narrowing have also been simulated, for the situation around the Maeslandt Barrier in the access channel to Rotterdam. Figure 4.51 shows that high flow velocities occur, due to the high ship speed combined with the narrow cross-section and the presence of shallow areas near the bank.

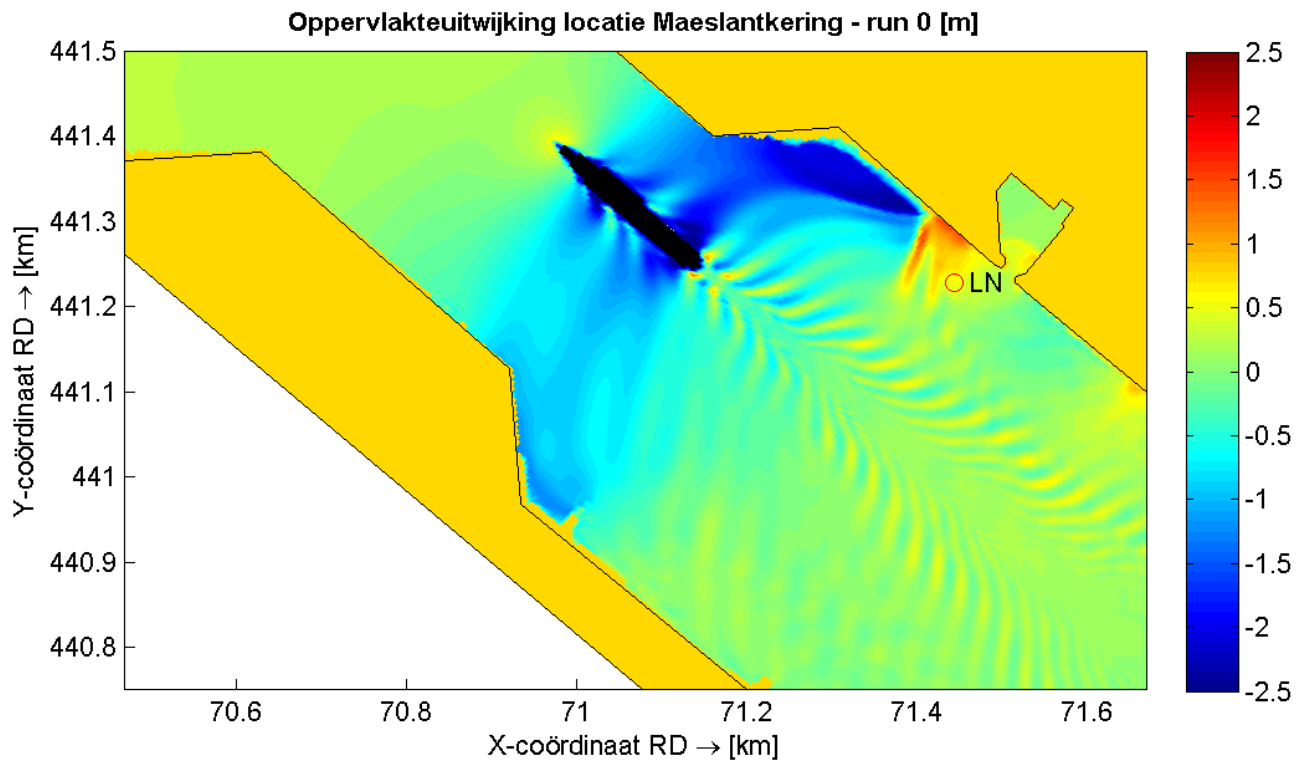


Figure 4.51: Flow field near the Maeslant barrier due to a ship passing a channel narrowing (Deltares, 2012).

Finally, we will show some examples of CFD results for flow velocities induced by propulsion systems. Figure 4.52 shows the flow field induced by a water jet directed towards the bed. Figure 4.53 shows the flow field in between a ship and the quay wall generated by a bow thruster.

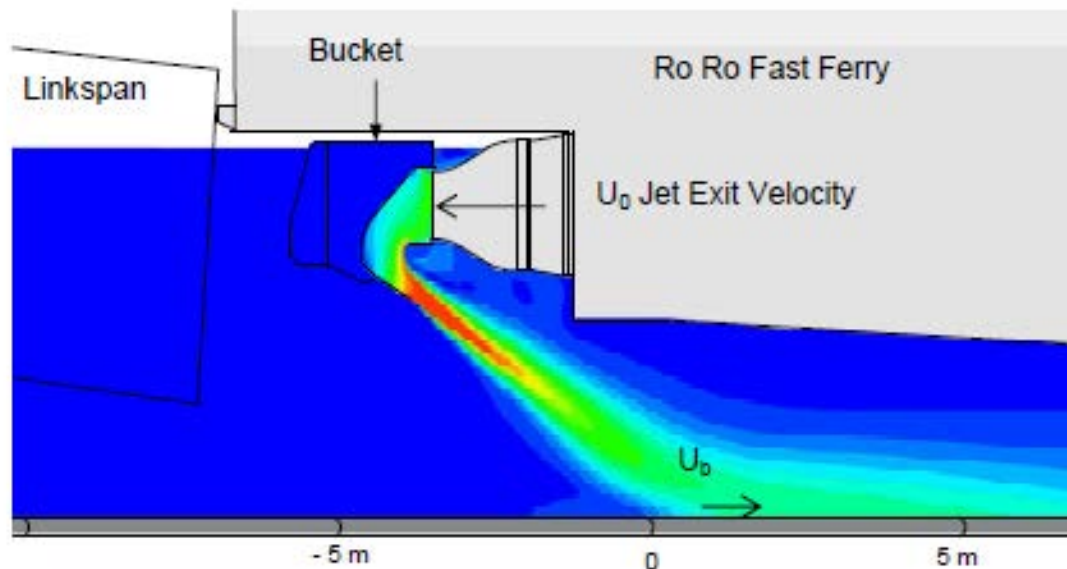


Figure 4.52: Flow field induced by a water jet (Hawkwood et al., 2013).

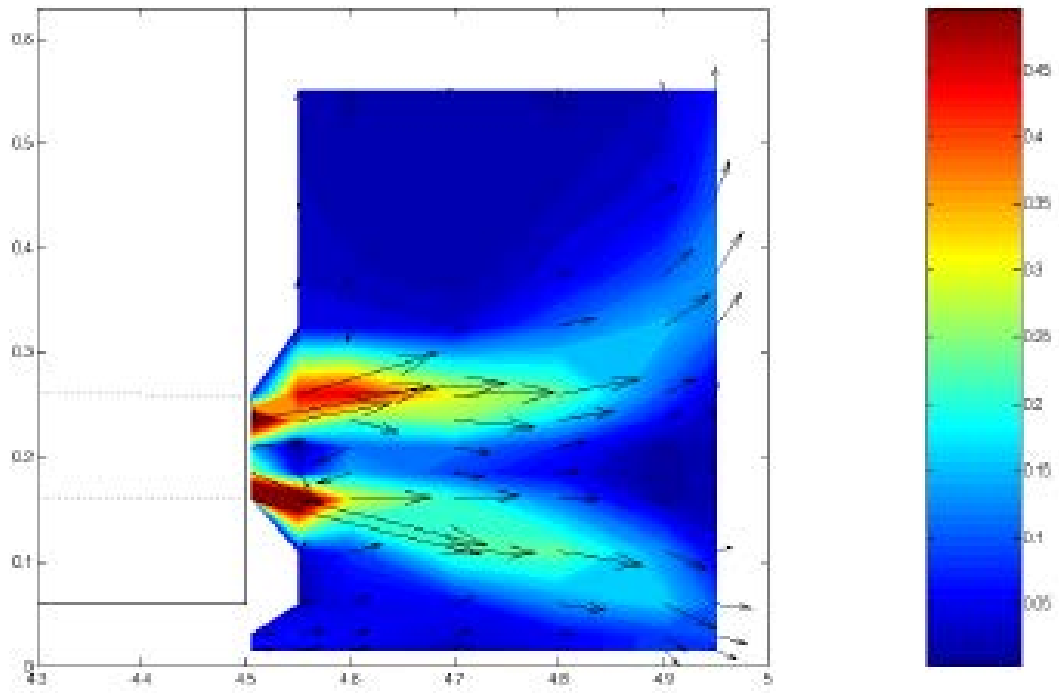


Figure 4.53: Flow field between ship and quay wall (Van Blaaderen, 2006).